Supporting Information

The spectroelectrochemical behaviour of redox-active manganese salen complexes

Marcello B. Solomon,[a] Bun Chan,[b] Clifford P. Kubiak,[c] Katrina A. Jolliffe,*[a] Deanna M. D'Alessandro*[a]

[a] School of Chemistry, The University of Sydney, New South Wales 2006, Australia, Fax: +61 2 9351 3329; Tel: +61 2 9351 3777; E-mail: deanna.dalessandro@sydney.edu.au; kate.jolliffe@sydney.edu.au

[b] Graduate School of Engineering, Nagasaki University, Bunkyo 1-14, Nagasaki-shi, Nagasaki 852-8521, Japan.

[c] Department of Chemistry and Biochemistry, University of California, San Diego, California 92093, United States

Table of Contents

Synthesis

General: Solution state ^{1}H and $^{13}C\{^{1}H\}$ NMR spectra were recorded on a Bruker AVANCE300, AVANCE400 or AVANCE500 spectrometer operating at 300, 400, 500 MHz for ^{1}H and 75, 100, 125 MHz for ^{13}C, respectively. ^{1}H and ^{13}C NMR chemical shifts were referenced internally to residual solvent resonances. Spectra were recorded at 298 K and chemical shifts (δ), with uncertainties of ± 0.01 Hz for ^{1}H and ± 0.05 Hz for ^{13}C are quoted in ppm. Coupling constants (J) are quoted in Hz and have uncertainties of ± 0.05 Hz for ^{1}H-^{1}H. Deuterated solvents were obtained from Cambridge Stable Isotopes and used as received. Low resolution electrospray ionization (ESI) mass spectra were acquired as a solution in acetonitrile, methanol or DMF with a 100 μL/min flow rate on a Finnegan LCQ or amazon MS detector. Spectra were collected over the mass range m/z 100 to 1000. An ESI spray voltage of 5 kV was applied with a heated capillary temperature of 200 °C and a nitrogen sheath gas pressure of 60 psi. Melting points were measured using a Gallenkamp melting point apparatus with the sample placed in a glass capillary and are uncorrected.

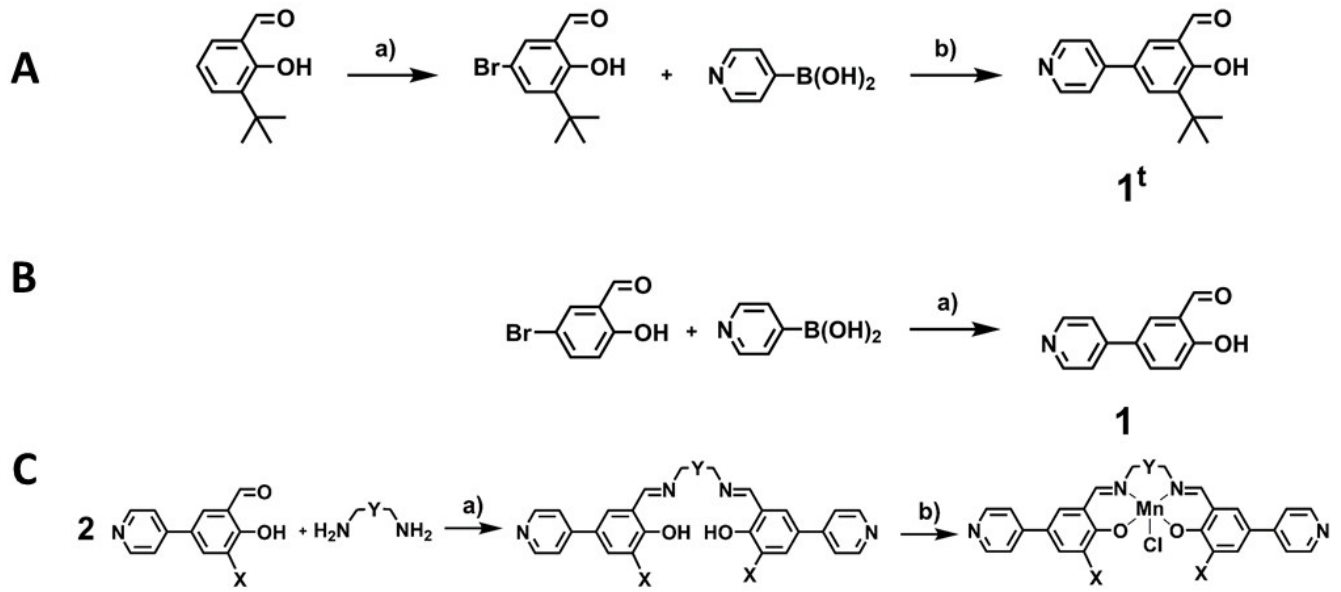

Scheme S1. A Synthesis of 3-*tert*-butyl-2-hydroxy-5-(4-pyridinyl) benzaldehyde (1^{t}). **a)** 5 eq. Br_2, solvent: CH_3COOH, r.t., 2 h **b)** catalyst: $[Pd(PPh_3)_4]$ (9 mol%), base: Na_2CO_3 (1.5 eq.), solvent: DME/H_2O (2:1), 100 °C, 16 h. **B** Synthesis of 2-hydroxy-5-(4-pyridinyl) benzaldehyde (1) **a)** catalyst: $[Pd(PPh_3)_4]$ (10 mol%), base: Cs_2CO_3 (2 eq.), solvent: toluene/ethanol, 105 °C, 8 h. **C** Synthetic routes to pyridyl terminated salens and their metal complexes **a)** solvent: methanol, 80 °C, 2 h. **b)** $Mn(OAc)_2 \cdot 4H_2O$ (1.1 eq.) under N_2, followed by LiCl (4.eq.) in air, solvent: ethanol (10 mL), r.t, 48 h.

5-Bromo-3-*tert*-butyl-2-hydroxybenzaldehyde. Elemental bromine (4.00 mL, 156 mmol) was added to glacial acetic acid (6 mL) and stirred. The solution was added dropwise to 3-*tert*-butyl-2-hydroxybenzaldehyde (5.00 g, 28.1 mmol) and the reaction was stirred for 2 h. The mixture was diluted in dichloromethane (150 mL), washed with saturated aqueous $Na_2S_2O_5$ (3 × 50 mL), saturated aqueous $NaHCO_3$ (3 × 50 mL) and saturated aqueous NaCl (3 × 50 mL). The organic layer was dried over Na_2SO_4 and the solvent removed to yield the product as a yellow solid (Yield: 6.68 g, 93%). **M.P.** 58–59 °C (lit.[1] 58–60 °C) **^{1}H NMR** (200 MHz, $CDCl_3$) δ (ppm) 11.72 (s, 1H), 9.80 (s, 1H), 7.57 (d, $^{4}J_{H\text{-}H}$ = 2.6 Hz, 1H), 7.51 (d, $^{4}J_{H\text{-}H}$ = 2.6 Hz, 1H), 1.40 (s, 9H). The characterisation data matched that reported in the literature.[1]

2-Hydroxy-5-(4-pyridinyl)-benzaldehyde (1). A solution of toluene and ethanol (4:1, 25 mL) was degassed with N_2 for 30 min. Under N_2, 5-bromo-2-hydroxybenzaldehyde (0.250 g, 1.24 mmol), Cs_2CO_3 (0.800 g, 2.46 mmol), (4-pyridinyl)-boronic acid (0.180 g, 1.47 mmol) and [$Pd(PPh_3)_4$] (0.135 g, 0.117 mmol) were combined and stirred under N_2 away from light for 10 min, before being heated at 105 °C for 4 h under N_2. Extra Cs_2CO_3 (0.200 g, 0.615 mmol), 4-(pyridinyl)-boronic acid (0.045 g, 0.368 mmol) and [$Pd(PPh_3)_4$] (0.034 g, 0.029 mmol) were added and the reaction progressed for a further 4 h. The solution was filtered through Celite and washed first with toluene, until the washings went colourless, then with methanol, until the washings went colourless. The solvent was removed from the methanol layer and the residue set aside. The toluene layer was washed with a solution of NaOH (3 × 40 mL), neutralised and then extracted into ethyl acetate (4 × 50 mL). The organic layer was washed with aqueous saturated NaCl (4 × 50 mL) and dried over Na_2SO_4. The solvent was evaporated and added to the crude residue from the methanol layer. The combined crude residues were purified *via* chromatography (SiO_2, ethyl acetate/hexane (2:1)) to afford the product as a light yellow powder (Yield: 0.178 g, 72%). **M.P.** 169–170 °C (lit.[2] 170–171 °C) **^{1}H NMR** (200 MHz, $CDCl_3$) δ (ppm) 11.14 (s, 1H), 10.01 (s, 1H), 8.67 (d, $^3J_{H\text{-}H}$ = 4.6 Hz, 2H), 7.83 (dd, $^3J_{H\text{-}H}$ = 7.8 Hz, $^4J_{H\text{-}H}$ = 4.7 Hz, 1H) , 7.48 (d, $^3J_{H\text{-}H}$ = 4.6 Hz, 2H), 7.13 (d, $^3J_{H\text{-}H}$ = 8 Hz, 1 H) The characterisation data matched that reported in the literature.[2]

3-*tert*-Butyl-2-hydroxy-5-(4-pyridinyl)-benzaldehyde (1^t). A solution of 1,2-dimethoxyethane and H_2O (3:1, 32 mL) was degassed with N_2 for 20 minutes. Under N_2, 5-bromo-3-*tert*-butyl-2-hydroxybenzaldehyde (0.510 g, 1.99 mmol), Na_2CO_3 (0.318 g, 3.00 mmol), (4-pyridinyl)-boronic acid (0.254 g, 2.06 mmol) and [$Pd(PPh_3)_4$] (0.200 g, 0.173 mmol) were added and the reaction stirred away from light for 10 min before being heated at 100 °C for 16 h. The black mixture was cooled to room temperature prior to the addition of H_2O (100 mL) for 30 min. The product was extracted into ethyl acetate (4 × 75 mL). The organic layers were combined, washed with aqueous saturated NaCl (3 × 30 mL) and dried over Na_2SO_4. The solvent was removed and the crude oil was purified *via* chromatography (SiO_2, ethyl acetate/hexane (2:1)) to afford the product as a yellow oil (Yield: 0.334 g, 66%). **^{1}H NMR** (200 MHz, $CDCl_3$) δ (ppm) 11.93 (s, 1H), 9.98 (s, 1H), 8.67 (d, $^3J_{H\text{-}H}$ = 6.2 Hz, 2H), 7.80 (d, $^4J_{H\text{-}H}$ = 1.6 Hz, 1H), 7.69 (d, $^4J_{H\text{-}H}$ = 1.6 Hz, 1H), 7.48 (d, $^3J_{H\text{-}H}$ = 6 Hz, 2H), 1.48 (s, 9H). The characterisation data matched that reported in the literature.[3]

General synthesis for salen complexes. The salen precursor (2 eq.) was suspended in methanol under an N_2 atmosphere. The diamine (~ 1 eq.) was added dropwise as a liquid, or added as a solid, before the mixture was heated at 80 °C for 2 h. The reaction was cooled on ice. If the product was a solid, it was separated *via* centrifugation, washed with cold methanol, cold diethyl ether and dried. If the product was an oil, the solvent was evaporated, and the product washed with ethyl acetate, or purified *via* chromatography (SiO_2, ethyl acetate).

3,3'-[1,2-Ethanediyl*bis*(nitromethylidine) *bis*[2-hydroxy-5-(4-pyridinyl)-benzaldehyde] (P1). 1 (0.094 g, 0.472 mmol) was dissolved in methanol (5 mL). A solution of 1,2-ethanediamine (15 µL, 0.236 mmol) in methanol (3 mL) was added dropwise and the solution turned bright yellow. The reaction progressed according to the general procedure to afford the product as a bright yellow powder, which was washed with cold methanol (3 × 1 mL), diethyl ether (3 × 1 mL) and dried (Yield: 0.084 g, 84%). **M.P.** 137 °C **^{1}H NMR (500 MHz, d_6-DMSO)** δ (ppm) 13.74 (s, 1H), 8.71 (s, 1H), 8.57 (dd, $^3J_{H\text{-}H}$ = 4.2 Hz, $^4J_{H\text{-}H}$ = 1.6 Hz, 2H), 7.97 (d, $^4J_{H\text{-}H}$ = 2.2 Hz, 1H), 7.80 (dd, $^3J_{H\text{-}H}$ = 8.6 Hz, $^4J_{H\text{-}H}$ = 2.2 Hz, 1H), 7.65 (dd, $^3J_{H\text{-}H}$ = 4.2 Hz, $^4J_{H\text{-}H}$ = 1.6 Hz, 2H), 6.99 (d, $^3J_{H\text{-}H}$ = 9 Hz, 1H), 4.00 (s, 2H); **^{13}C{^{1}H} NMR (125 MHz, d_6-DMSO)** δ (ppm) 166.8, 162.2, 150.1, 146.0, 130.8, 130.1, 127.0, 120.3, 118.7, 117.7, 48.5 **ATR-IR (cm^{-1})** $\nu_{O\text{-}C(Ph)}$ = 1640, $\nu_{C=N}$ = 1594 **UV-Vis-NIR λ(KBr, cm^{-1})** 23050, 29200 (sh), 30950, 37501 **MS (ESI+, methanol)** *m/z*

calculated for $C_{26}H_{22}N_4O_2$ $[M+H]^+$: 423.17, found: 423.16 **Elemental Analysis** calculated for $C_{26}H_{22}N_4O_2$: C 73.9, H 5.3, N 13.3%, found C 73.5, H 5.1, N 13.0%.

3,3'-[1,2-Ethanediyl*bis*(nitromethylidine)] *bis*[3-*tert*-butyl-2-hydroxy-5-(4-pyridinyl)-benzaldehyde] (^{t}P1). 1^t (0.636 g, 2.49 mmol) was dissolved in methanol (35 mL). A solution of 1,2-ethanediamine (83 µL, 1.24 mmol) in methanol (5 mL) was added dropwise and the solution turned bright yellow. The reaction progressed according to the general procedure to afford the product as a bright yellow powder, which was washed with cold methanol (3 × 5 mL) and dried under vacuum overnight (Yield: 0.607 g, 92%). **M.P.** 229–230 °C **^{1}H NMR (400 MHz, $CDCl_3$):** δ 14.11 (s, 1H), 8.60 (dd, *J*= 1.6 Hz, 4.4 Hz, 2H), 8.48 (s, 1H), 7.60 (d, *J*= 2.4 Hz, 1H), 7.43 (dd, *J*= 1.6 Hz, 4.4 Hz, 2H), 7.39 (d, *J*= 2.4 Hz, 1H), 4.02 (s, 2H), 1.47 (s, 9H); **^{13}C{^{1}H} NMR (100 MHz, $CDCl_3$)** δ 167.1, 161.5, 150.2, 148.0, 138.6, 128.2, 128.2, 127.6, 120.9, 118.8, 59.2, 35.1, 29.3; **ATR-IR (cm^{-1})** $\nu_{O\text{-}C(Ph)}$ = 1630 $\nu_{C=N}$ = 1591 **UV-Vis-NIR: λ_{max}(KBr), cm^{-1})** 19013, 25518, 31069,8163 (sh); **MS (ESI+, methanol):** *m/z* calculated for $C_{34}H_{38}N_4O_2$ $[M+H]^+$: 535.30, found: 535.20; **Elemental Analysis** calculated for $C_{34}H_{38}N_4O_2$: C 76.4, H 7.2, N 10.5%, found: C 76.1, H 7.3, N 10.4%.

3,3'-[(1R,2R)-Diaminocyclohexanediyl*bis*(nitromethylidine) *bis*[2-hydroxy-5-(4-pyridinyl)-benzaldehyde (P2). 1 (0.130 g, 0.653 mmol) was dissolved in methanol (10 mL). A solution of (1*R*,2*R*)-diaminocyclohexane (39 µL, 0.323 mmol) in methanol (5 mL) was added dropwise and the solution turned bright yellow. The reaction progressed according to the general procedure to afford the product as a bright yellow powder, which was washed with cold methanol (3 × 2 mL), diethyl ether and dried (Yield: 0.109 g, 71%). **M.P.** 119–121 °C **^{1}H NMR (400 MHz, MeOD)** δ (ppm) 8.43 (d, $^3J_{H\text{-}H}$ = 5.7 Hz, 2H), 8.42 (s, 1H), 7.61–7.56 (m, 2H), 7.47 (d, $^3J_{H\text{-}H}$ = 5.7 Hz, 2H), 6.88 (dd, $^3J_{H\text{-}H}$ = 9.2 Hz, $^4J_{H\text{-}H}$ = 2.1 Hz, 2H), 3.46 (m, 1H), 2.05 (m, 1H), 1.92 (m, 1H), 1.78 (m, 1H), 1.56 (m, 1H) **^{13}C{^{1}H} NMR (100 MHz, MeOD)** δ (ppm) 166.8, 165.1, 150.3, 149.4, 132.3, 131.6, 128.5, 122.1, 119.9, 119.3, 73.0, 33.8, 25.2 **ATR-IR (cm^{-1})** $\nu_{O\text{-}C(Ph)}$ = 1626, $\nu_{C=N}$ = 1589 **UV-Vis-NIR λ(KBr, cm^{-1})** 23118, 24166, 30085 (sh), 34411 (sh), 38689 **MS (ESI+, methanol)** *m/z* calculated for $C_{30}H_{28}N_2O_4$ $[M+H]^+$: 477.22, found: 477.26 **Elemental Analysis** calculated for $C_{30}H_{28}N_2O_4$: C 75.6, H 5.9, N 11.8%, found C 75.9, H 5.5, N 11.7%.

3,3'-[(1R,2R)-Diaminocyclohexanediyl*bis*(nitromethylidine)*bis*[3-*tert*-Butyl2-hydroxy-5-(4-pyridinyl)-benzaldehyde (^{t}P2). 1^t (0.392 g, 1.54 mmol) was dissolved in methanol (25 mL). A solution of (1*R*,2*R*)-diaminocyclohexane (91 µL, 0.758 mmol) in methanol (5 mL) was added dropwise and the solution turned bright yellow. The reaction progressed according to the general procedure to afford the product as a bright yellow oil, which was purified *via* chromatography (SiO_2, ethyl acetate) (Yield: 0.331 g, 74%) **M.P.** 211–213 °C (lit.[4] 212–213 °C) **^{1}H NMR (300 MHz, $CDCl_3$)** δ (ppm) 8.57 (dd, $^3J_{H\text{-}H}$ = 5.4 Hz, $^4J_{H\text{-}H}$ = 1.6 Hz, 2H), 8.34 (s, 1H), 7.51 (d, $^4J_{H\text{-}H}$ = 1.8 Hz, 1H), 7.36 (dd, $^3J_{H\text{-}H}$ = 5.4 Hz, $^4J_{H\text{-}H}$ = 1.6 Hz, 2H), 7.27 (d, $^4J_{H\text{-}H}$ = 1.8 Hz, 1H), 3.45 (m, 1H), 2.10–1.48 (m, 4H), 1.44 (s, 9H). The characterisation data matched that reported in the literature.[5]

3,3'-[Phenylenediyl*bis*(nitromethylidine)] *bis*[2-hydroxy-5-(4-pyridinyl)-benzaldehyde] (P3). 1 (0.095 g, 0.477 mmol) was dissolved in methanol (5 mL). *o*-Phenylenediamine (0.025 g, 0.239 mmol) was added as a solid and the solution turned bright orange. The reaction progressed according to the general procedure to afford the product as a bright orange powder, which was washed with cold methanol (3 × 2 mL) and dried (Yield: 0.075 g, 67%). **M.P.** 227–229 °C **^{1}H NMR (500 MHz, d_6-DMSO)** δ (ppm) 13.44 (s, 1H), 8.66 (dd, $^3J_{H\text{-}H}$ = 4.2 Hz, $^4J_{H\text{-}H}$ = 1.4 Hz, 2H), 8.61 (d, $^4J_{H\text{-}H}$ = 2 Hz, 1H), 7.89 (dd, $^3J_{H\text{-}H}$ = 8.8 Hz, $^4J_{H\text{-}H}$ = 2.4 Hz, 1H), 7.78 (dd, $^3J_{H\text{-}H}$ = 4.2 Hz, $^4J_{H\text{-}H}$ = 1.4 Hz, 2H), 7.69–7.74 (m, 1H), 7.30–7.34 (m, 1H), 7.19 (d, $^3J_{H\text{-}H}$ = 8.6 Hz, 1H); **^{13}C{^{1}H} NMR (125 MHz, d_6-DMSO)** δ (ppm)

159.1, 151.4, 150.2, 146.1, 131.5, 129.9, 128.8, 127.8, 124.7, 123.1, 120.4, 118.1, 113.2 **ATR-IR (cm^{-1})** $\nu_{O\text{-}C(Ph)}$ = 1622, $\nu_{C=N}$ = 1592 **UV-Vis-NIR λ(KBr, cm^{-1})** 19454 (sh), 20795, 25766 (sh), 28851, 32626 (sh), 37796 (sh) **MS (ESI+, methanol)** *m/z* calculated for $C_{30}H_{22}N_4O_2$ $[M+H]^+$: 471.53, found: 471.53 **Elemental Analysis** calculated for $C_{30}H_{22}N_4O_2$: C 76.6, H 4.7, N 11.9%, found C 76.6, H 4.9, N 11.7%.

3,3'-[Phenylenediyl*bis*(nitromethylidine)] *bis*[3-*tert*-butyl-2-hydroxy-5-(4-pyridinyl)-benzaldehyde] (^{t}P3). 1^t (0.544 g, 2.13 mmol) was dissolved in methanol (30 mL). *o*-Phenylenediamine (0.115 g, 1.06 mmol) added as a solid and the solution turned bright orange. The reaction progressed according to the general procedure to afford the product as a bright orange solid, which was washed with cold methanol (3 × 5 mL), and dried (Yield: 0.567 g, 0.973 mmol, 92%). **M.P.** 270 °C (lit.[4] 268–269 °C) **^{1}H NMR (300 MHz, MeOD)** δ (ppm) 8.97 (s, 1H), 8.54 (dd, $^3J_{H\text{-}H}$ = 5.8 Hz, $^4J_{H\text{-}H}$ = 1.4 Hz, 2H), 7.86 (d, $^4J_{H\text{-}H}$ = 1.8 Hz), 7.77 (d, $^4J_{H\text{-}H}$ = 1.8 Hz), 7.71 (dd, $^3J_{H\text{-}H}$ = 5.8 Hz, $^4J_{H\text{-}H}$ = 1.4 Hz, 2H), 7.52–7.42 (m, 2H), 1.48 (s, 9H). The characterisation data matched that reported in the literature.[6]

3,3'-[4,5-Dimethyl-phenylenediyl*bis*(nitromethylidine)] *bis*[2-hydroxy-5-(4-pyridinyl)-benzaldehyde] (P4). 1 (0.130 g, 0.653 mmol) was dissolved in methanol (10 mL). 4,5-dimethyl-*o*-phenylenediamine (0.044 g, 0.327 mmol) was added as a solid and the solution turned bright orange. The reaction progressed according to the general procedure to afford the product as a bright orange powder, which was washed with cold methanol (3 × 5 mL) and dried (Yield: 0.124 g, 76%). **M.P.** 243–244 °C **^{1}H NMR (400 MHz, d_6-DMSO) δ (ppm)** 13.46 (s, 1H), 9.09 (s, 1H), 8.62 (dd, $^3J_{H\text{-}H}$ = 4.3 Hz, $^4J_{H\text{-}H}$ = 1.5 Hz, 2H), 8.27 (d, $^4J_{H\text{-}H}$ = 1.5 Hz, 1H), 7.90 (dd, $^3J_{H\text{-}H}$ = 8.8 Hz, $^4J_{H\text{-}H}$ = 2.4 Hz, 1H), 7.73 (dd, $^3J_{H\text{-}H}$ = 4.3 Hz, $^4J_{H\text{-}H}$ = 1.5 Hz, 2H), 7.37 (s, 1H), 7.11 (d, $^3J_{H\text{-}H}$ = 8.8 Hz, 1H), 2.33 (s, 3H) **^{13}C{^{1}H} NMR (100 MHz, d_6-DMSO)** δ (ppm) 161.8, 161.4, 150.2, 146.0, 139.4, 136.6, 131.4, 130.1, 127.4, 120.3, 120.2, 119.9, 117.8, 19.2 **ATR-IR (cm^{-1})** $\nu_{O\text{-}C(Ph)}$ = 1617, $\nu_{C=N}$ = 1583 **UV-Vis-NIR λ(KBr, cm^{-1})** 19443 (sh), 20504, 23134 (sh), 26291, 29164, 33582, 36701 **MS (ESI+, methanol)** *m/z* calculated for $C_{32}H_{26}N_4O_2$ $[M+H]^+$: 499.21, found: 499.24 **Elemental Analysis** calculated for $C_{32}H_{26}N_4O_2$: C 77.1, H 5.3, N 11.2%, found C 77.3, H 5.1, N 11.5%.

3,3'-[4,5-Dimethyl-phenylenediyl*bis*(nitromethylidine)]*bis*[3-*tert*-butyl-2-hydroxy-5-(4-pyridinyl)-benzaldehyde] (^{t}P4). 1^t (0.185 g, 0.725 mmol) and 4,5-dimethyl-*o*-phenylenediamine (0.050 g, 0.367 mmol) were dissolved in methanol (15 mL), which formed a bright orange solution. The reaction progressed according to the general procedure to afford the product as a bright orange powder, which was washed with cold methanol (3 × 3 mL) and dried (Yield: 0.183 g, 82%). **M.P.** 282–285 °C **^{1}H NMR (400 MHz, $CDCl_3$):** δ 14.16 (s, 1H), 8.78 (s, 1H), 8.63 (dd, *J*= 1.6 Hz, 4.4 Hz, 2H), 7.67 (d, *J*= 2.4 Hz, 1H), 7.56 (d, *J*= 2.4 Hz, 1H) 7.49 (dd, *J*= 1.6 Hz, 4.4 Hz, 2H), 7.12 (s, 1H), 2.36 (s, 3H), 1.48 (s, 9H); **^{13}C{^{1}H} NMR (100 MHz, $CDCl_3$)** δ 163.1, 161.8, 150.2, 148.0, 139.6, 138.9, 136.7, 129.0, 128.8, 127.8, 121.0, 120.8, 119.5, 35.2, 29.3, 19.6, 18.4; **ATR-IR (cm^{-1})** $\nu_{O\text{-}C(Ph)}$ = 1612, $\nu_{C=N}$ = 1593 **UV-vis-NIR: λ(KBr, cm^{-1})** 18557 (sh), 19698, 24579, 33751, 35895 (sh); **MS (ESI+, methanol)** *m/z* calculated for $C_{40}H_{42}N_4O_2$ [M+H]: 611.33, found: 611.20; **Elemental Analysis** calculated for $C_{40}H_{42}N_4O_2$: C 78.7, H 6.9, N 9.2%, found: C 78.4 H 7.0, N 9.1%.

General synthesis for the metalation of salen complexes. A solution of salen (1 eq.) in ethanol was degassed with N_2 and stirred for 10 min. $Mn(OAc)_2$•$4H_2O$ (1.1 eq.) was added and the reaction stirred overnight under N_2. The reaction was removed from N_2, LiCl (4 eq.) was added and the reaction stirred in air overnight. The excess ethanol was removed and the residue washed with H_2O and dried overnight *in vacuo*.

3,3'-[1,2-Ethanediyl*bis*(nitromethylidine)*bis*[2-hydroxy-5-(4-pyridinyl)-benzaldehyde]Manganese(III) chloride (MnP1Cl). P1 (0.100 g, 0.237 mmol) was dissolved in degassed ethanol (10 mL). $Mn(OAc)_2$•$4H_2O$ (0.064 g,

0.261 mmol) and LiCl (0.045 g, 1.06 mmol) were added and reacted according to the general procedure to obtain the solid as a dark brown powder, which was washed with H_2O, until the washings were colourless and dried (Yield: 0.112 g, 92%). **M.P.** > 350 °C **ATR-IR (cm^{-1}):** $\nu_{O\text{-}C(Ph)}$ = 1628, $\nu_{C=N}$ = 1597 **UV-Vis-NIR λ(KBr, cm^{-1})** 16200, 19500, 24570, 28000, 31360, 37060 **MS (ESI+, methanol)** *m/z* calculated for $C_{26}H_{20}MnN_4O_2$ $[M\text{-}Cl]^+$: 475.10, found: 475.07 **Elemental Analysis** calculated for $C_{26}H_{20}ClMnN_4O_2$: C 60.5, H 4.5, N 10.8%, found C 60.3, H 4.9, N 10.4%.

3,3'-[1,2-Ethanediyl*bis*(nitromethylidine)]*bis*[3-*tert*-butyl-2-hydroxy-5-(4-pyridinyl)-benzaldehyde] Manganese(III) chloride (Mn^{t}P1Cl). ^{t}P1 (0.607 g, 1.14 mmol) was suspended in degassed ethanol (20 mL). $Mn(OAc)_2$•$4H_2O$ (0.306 g, 1.25 mmol) and LiCl (0.212 g, 5.00 mmol) were added and reacted according to the general procedure to obtain the solid as a dark brown powder, which was washed with H_2O, until the washings were colourless, and dried (Yield: 0.594 g, 84%). **M.P.** > 350 °C **ATR-IR (cm^{-1})** $\nu_{O\text{-}C(Ph)}$ = 1625, $\nu_{C=N}$ = 1599 **UV-Vis-NIR λ(KBr, cm^{-1})** 15860, 20610(sh), 23330, 27320, 30810, 39330 **MS (ESI+, methanol/DMF)** *m/z* calculated for $C_{34}H_{36}MnN_4O_2$ $[M\text{-}Cl]^+$: 587.22, found: 587.22 **Elemental Analysis** calculated for $C_{34}H_{36}ClMnN_4O_2$: C 65.5, H 5.8, N 9.0%, found C 65.1, H 6.0, N 8.7%.

[3,3'-[(1R,2R)-Diaminocyclohexanediyl*bis*(nitromethylidine)*bis*[2-hydroxy-5-(4-pyridinyl)-benzaldehyde] Manganese(III) chloride (MnP2Cl). P2 (0.153 g, 0.260 mmol) was dissolved in degassed ethanol (15 mL). $Mn(OAc)_2$•$4H_2O$ (0.070 g, 0.286 mmol) and LiCl (0.049 g, 1.14 mmol) were added and reacted according to the general procedure to obtain the solid as a dark brown powder, which was washed with H_2O, until the washings were colourless, and dried (Yield: 0.110 g, 75%). **M.P.** > 350 °C **ATR-IR (cm^{-1})** $\nu_{O\text{-}C(Ph)}$ = 1639, $\nu_{C=N}$ = 1597 **UV-Vis-NIR λ(KBr, cm^{-1})** 16070, 23710(sh), 27710, 32090(sh), 38690 **MS (ESI+, methanol)** *m/z* calculated for $C_{30}H_{26}MnN_4O_2$ $[M\text{-}Cl]^+$: 529.14, found: 529.18 **Elemental Analysis** calculated for $C_{30}H_{26}ClMnN_4O_2$•3ethanol: C 61.5, H 6.3, N 8.0%, found C 61.8, H 6.5, N 8.1%.

[3,3'-[(1R,2R)-Diaminocyclohexanediyl*bis*(nitromethylidine)*bis*[3-*tert*-Butyl2-hydroxy-5-(4-pyridinyl)-benzal dehyde] Manganese(III) chloride (Mn^{t}P2Cl). ^{t}P2 (0.331 g, 0.563 mmol) was dissolved in degassed ethanol (30 mL). $Mn(OAc)_2$•$4H_2O$ (0.207 g, 0.845 mmol) and LiCl (0.143 g, 3.37 mmol) were added and reacted according to the general procedure to obtain the solid as a dark brown powder, which was washed with H_2O, until the washings went colourless, and dried (Yield: 0.315 g, 83%). **M.P. >** 350 °C (lit.[5] > 350 °C). **UV-Vis-NIR: λ(KBr, cm^{-1})** 16010, 23950, 28010 (sh), 33160 **MS (ESI+, methanol)** *m/z* calculated for $C_{38}H_{42}MnN_4O_2$ $[M\text{-}Cl]^+$: 641.27, found: 641.36 **Elemental Analysis** calculated for $C_{38}H_{42}ClMnN_4O_2$•ethanol: C 66.5, H 6.6, N 7.8%, found C 66.2, H 6.9, N 7.9%. The characterisation data matched that reported in the literature.[5]

3,3'-[Phenylenediyl*bis*(nitromethylidine)]*bis*[2-hydroxy-5-(4-pyridinyl)-benzaldehyde] Manganese(III) chloride (MnP3Cl). P3 (0.120 g, 0.255 mmol) was dissolved in degassed ethanol (15 mL). $Mn(OAc)_2$•$4H_2O$ (0.069 g, 0.282 mmol) and LiCl (0.050 g, 1.18 mmol) were added and reacted according to the general procedure to obtain the solid as a dark brown powder, which was washed with H_2O, until the washings were colourless, and dried (Yield: 0.096 g, 67%). **M.P.** > 350 °C **ATR-IR (cm^{-1})** $\nu_{O\text{-}C(Ph)}$ = 1624, $\nu_{C=N}$ = 1597 **UV-Vis-NIR λ(KBr, cm^{-1})** 14170(sh), 17360(sh), 22190, 28350, 32070(sh) **MS (ESI+, methanol)** *m/z* calculated for $C_{30}H_{20}MnN_4O_2$ $[M\text{-}Cl]^+$: 523.10, found: 523.08 **Elemental Analysis** calculated for $C_{30}H_{20}ClMnN_4O_2$•ethanol: C 63.6, H 4.2, N 9.3%, found C 63.8, H 4.1, N 9.3%.

3,3'-[Phenylenediyl*bis*(nitromethylidine)]*bis*[3-*tert*-butyl-2-hydroxy-5-(4-pyridinyl)-benzaldehyde] Manganese(III) chloride (Mn^{t}P3Cl). ^{t}P3 (0.567 g, 0.974 mmol) was dissolved in degassed ethanol (40 mL).

$Mn(OAc)_2$•$4H_2O$ (0.262 g, 1.07 mmol) and LiCl (0.181 g, 4.26 mmol) were added and reacted according to the general procedure to obtain the solid as a dark brown powder, which was washed with H_2O, until the washings were colourless, and dried (Yield: 0.558 g, 85%). **M.P.** > 350 °C **ATR-IR (cm^{-1})** $\nu_{O\text{-}C(Ph)}$ = 1626, $\nu_{C=N}$ = 1594 **UV-Vis-NIR λ(KBr, cm^{-1})** 9570, 17950(sh), 24190, 27900, 31470(sh), 38600 **MS (ESI+, methanol)** *m/z* calculated for $C_{38}H_{36}MnN_4O_2$ $[M\text{-}Cl]^+$: 635.22, found: 635.22 **Elemental Analysis** calculated for $C_{38}H_{36}ClMnN_4O_2$•methanol: C 66.7, H 5.6, N 8.0%, found C 66.9, H 5.5, N 8.4%.

3,3'-[4,5-Dimethyl-phenylenediyl*bis*(nitromethylidine)]*bis*[2-hydroxy-5-(4-pyridinyl)-benzaldehyde] Manganese(III) chloride (MnP4Cl). P4 (0.075 g, 0.151 mmol) was dissolved in degassed ethanol (10 mL). $Mn(OAc)_2$•$4H_2O$ (0.041 g, 0.166 mmol) and LiCl (0.028 g, 0.624 mmol) were added and reacted according to the general procedure to obtain the solid as a dark brown powder, which was washed with H_2O until the washings were colourless, and dried (Yield: 0.064 g, 72%). **M.P.** > 350 °C **ATR-IR (cm^{-1})** $\nu_{O\text{-}C(Ph)}$ = 1617, $\nu_{C=N}$ = 1590 **UV-Vis-NIR λ(KBr, cm^{-1})** 14770(sh), 17820(sh), 24560, 39190 **MS (ESI+, methanol)** *m/z* calculated for $C_{32}H_{24}MnN_2O_4$ $[M\text{-}Cl]^+$: 551.13, found: 551.17 **Elemental Analysis** calculated for $C_{32}H_{24}ClMnN_2O_4$•ethanol: C 64.5, H 4.7, N 8.6%, found C 64.4, H 4.7, N 8.3%.

3,3'-[4,5-Dimethyl-phenylenediyl*bis*(nitromethylidine)]*bis*[3-*tert*-butyl-2-hydroxy-5-(4-pyridinyl)-benzaldehyde]Manganese(III) chloride (Mn^{t}P4Cl). ^{t}P4 (0.310 g, 0.532 mmol) was dissolved in degassed ethanol (35 mL). $Mn(OAc)_2$•$4H_2O$ (0.215 g, 0.877 mmol) and LiCl (0.125 g, 2.95 mmol) were added and reacted according to the general procedure to obtain the solid as a dark brown powder, which was washed with H_2O until the washings were colourless, and dried (Yield: 0.365 g, 98%). **M.P.** > 350 °C **ATR-IR (cm^{-1})** $\nu_{O\text{-}C(Ph)}$ = 1624, $\nu_{C=N}$ = 1583 **UV-Vis-NIR λ(KBr, cm^{-1})** 9490, 17290(sh), 24120, 27900, 32510(sh), 38150 **MS (ESI+, methanol)** *m/z* calculated for $C_{40}H_{40}MnN_4O_2$ $[M\text{-}Cl]^+$: 663.25, found: 663.25 **Elemental Analysis** calculated for $C_{40}H_{40}ClMnN_4O_2$•2ethanol: C 66.8, H 6.6, N 7.1%, found C 67.1, H 6.4, N 7.0%.

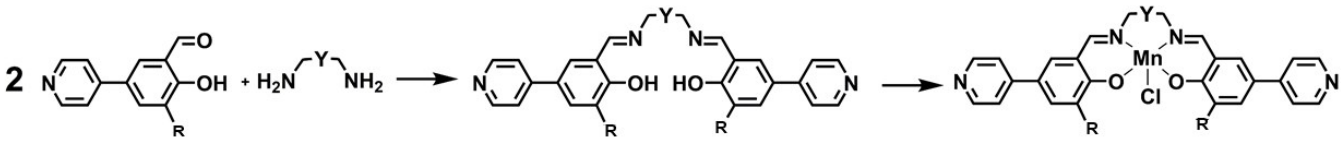

Free base yields

R \ Y				
H	P1 (84%)	P2 (71%)	P3 (67%)	P4 (76%)
	^{t}P1 (92%)	^{t}P2 (74%)	^{t}P3 (92%)	^{t}P4 (82%)

Metallated yields

R \ Y				
H	MnP1Cl (92%)	MnP2Cl (75%)	MnP3Cl (67%)	MnP4Cl (72%)
	Mn^{t}P1Cl (84%)	Mn^{t}P2Cl (83%)	Mn^{t}P3Cl (85%)	Mn^{t}P4Cl (98%)

Figure S1. Yields of free base and Mn(III) pyridyl salen complexes

Cyclic Voltammetry

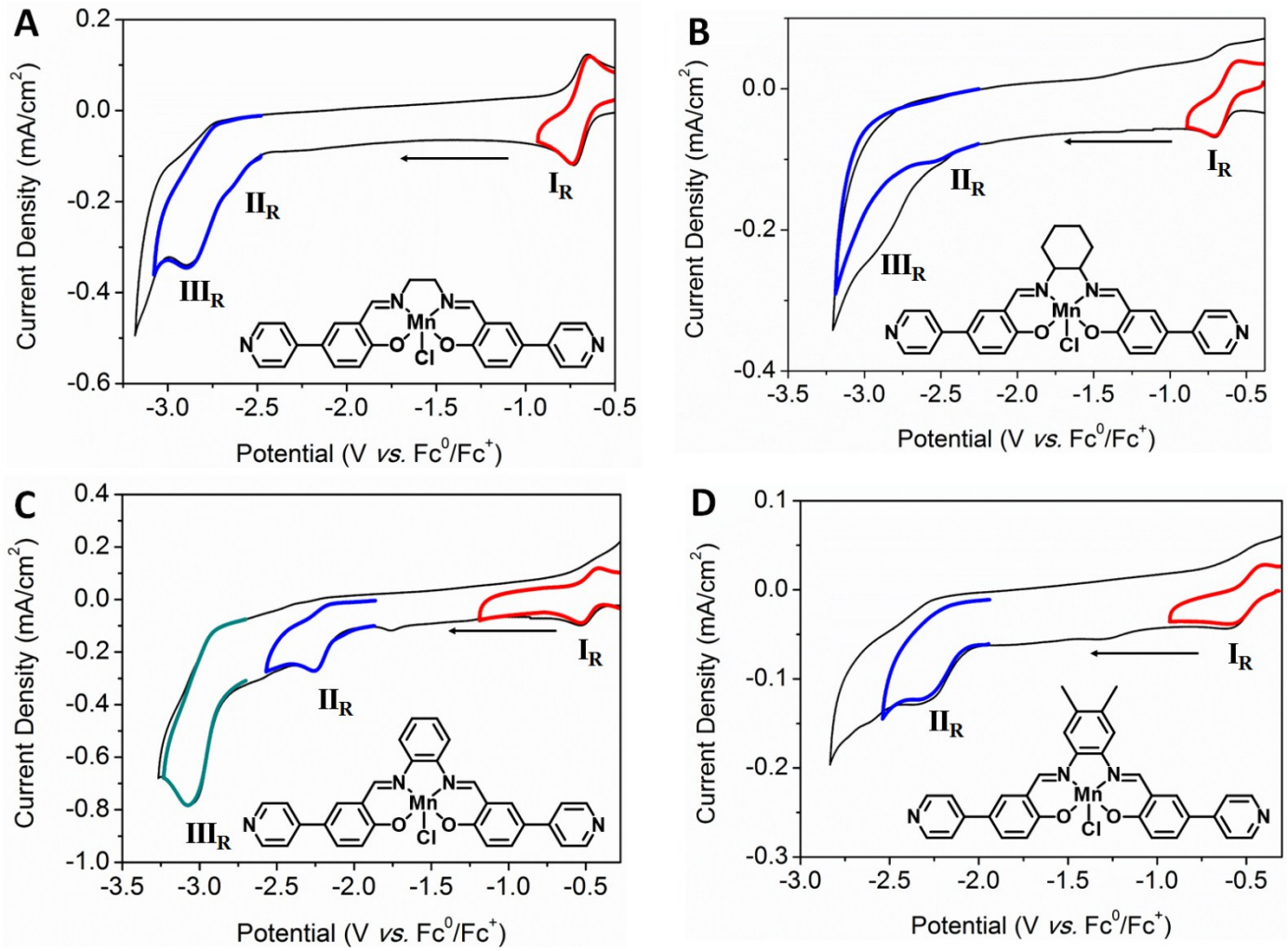

Figure S2. Solution state CV of **A MnP1Cl** (1 mM), **B MnP2Cl** (1 mM), **C MnP3Cl** (1 mM) and **D MnP4Cl** (1 mM). (0.1 M $[(n\text{-}C_4H_9)_4N]PF_6$/DMF as the supporting electrolyte under N_2, scan rate: 0.1 V s^{-1}, Fc (1 mM) was used as an internal standard). The I_R (red), II_R (blue) and III_R (green) processes were isolated.

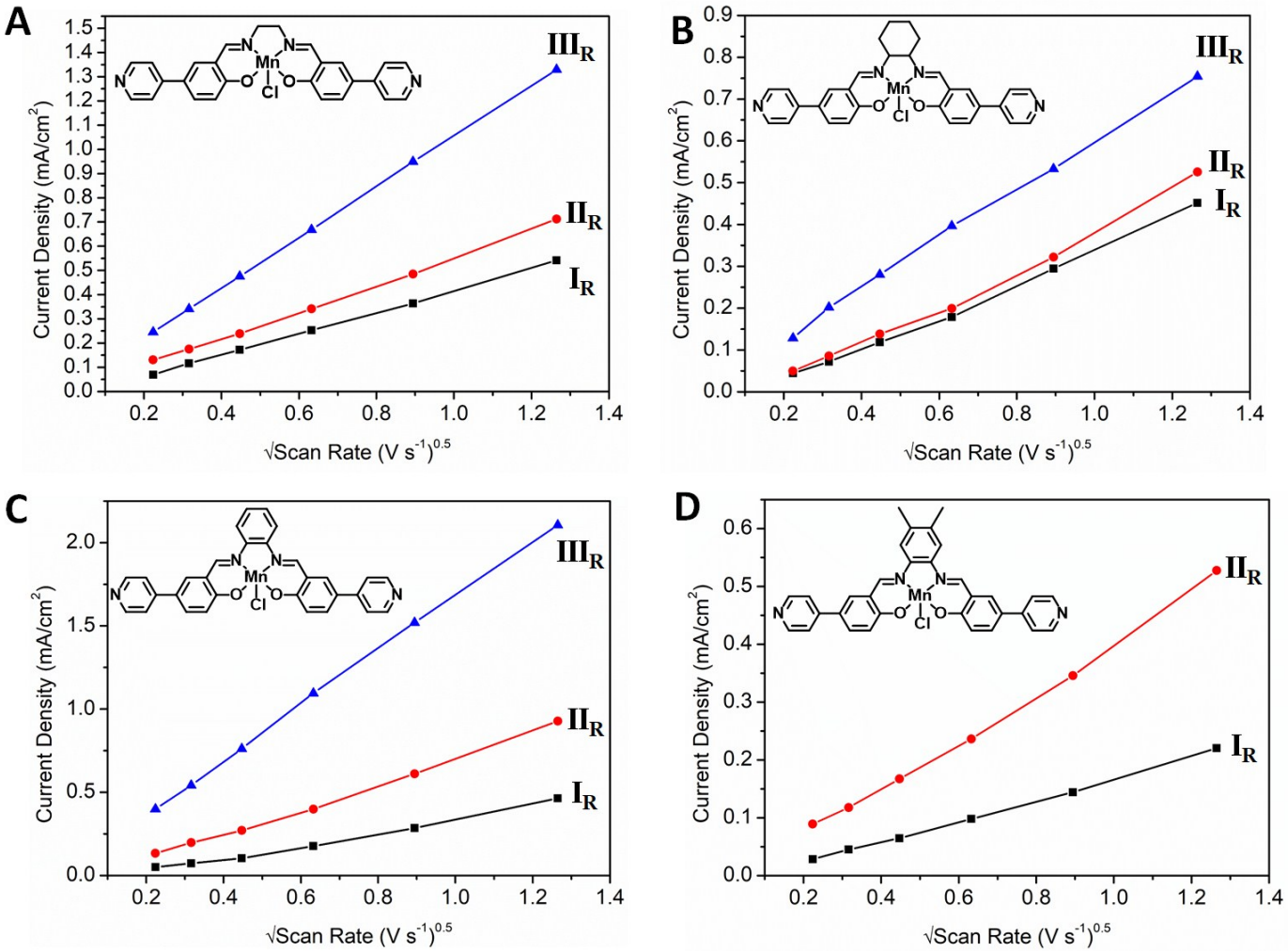

Figure S3. Scan rate dependence studies on each of the discrete salen complexes **A MnP1Cl** (1 mM), **B MnP2Cl** (1 mM), **C MnP3Cl** (1 mM) and **D MnP4Cl** (1 mM). (0.1 M $[(n\text{-}C_4H_9)_4N]PF_6$/DMF as the supporting electrolyte under N_2, Fc (1 mM) was used as an internal standard).

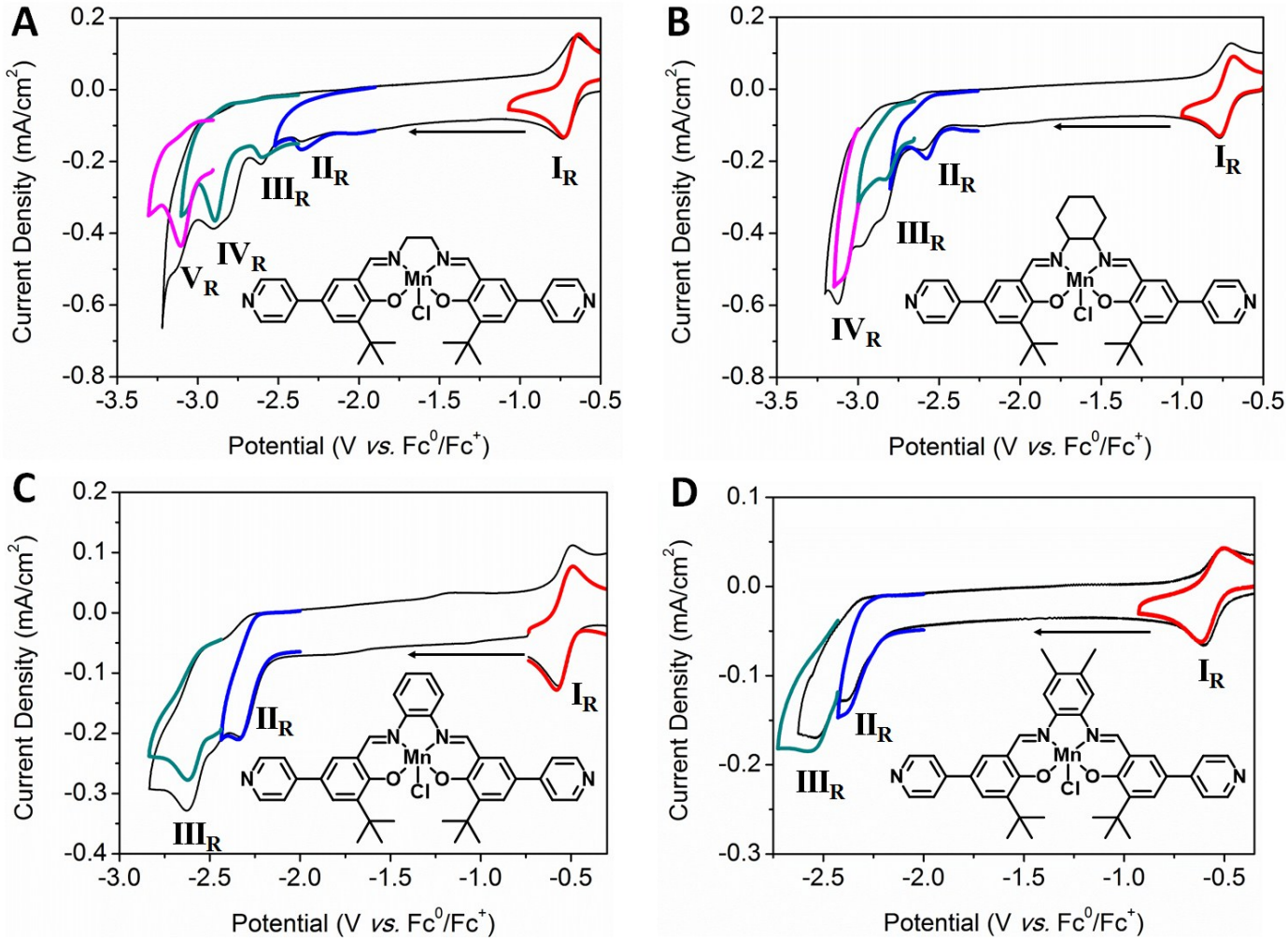

Figure S4. Solution state CV of **A Mn^{t}P1Cl** (1 mM), **B Mn^{t}P2Cl** (1 mM), **C Mn^{t}P3Cl** (1 mM) and **D Mn^{t}P4Cl** (1 Mm) (0.1 M $[(n\text{-}C_4H_9)_4N]PF_6$/DMF as the supporting electrolyte under N_2, scan rate: 0.1 V s^{-1}, Fc (1 mM) was used as an internal standard). The different colour traces represent the individual redox processes.

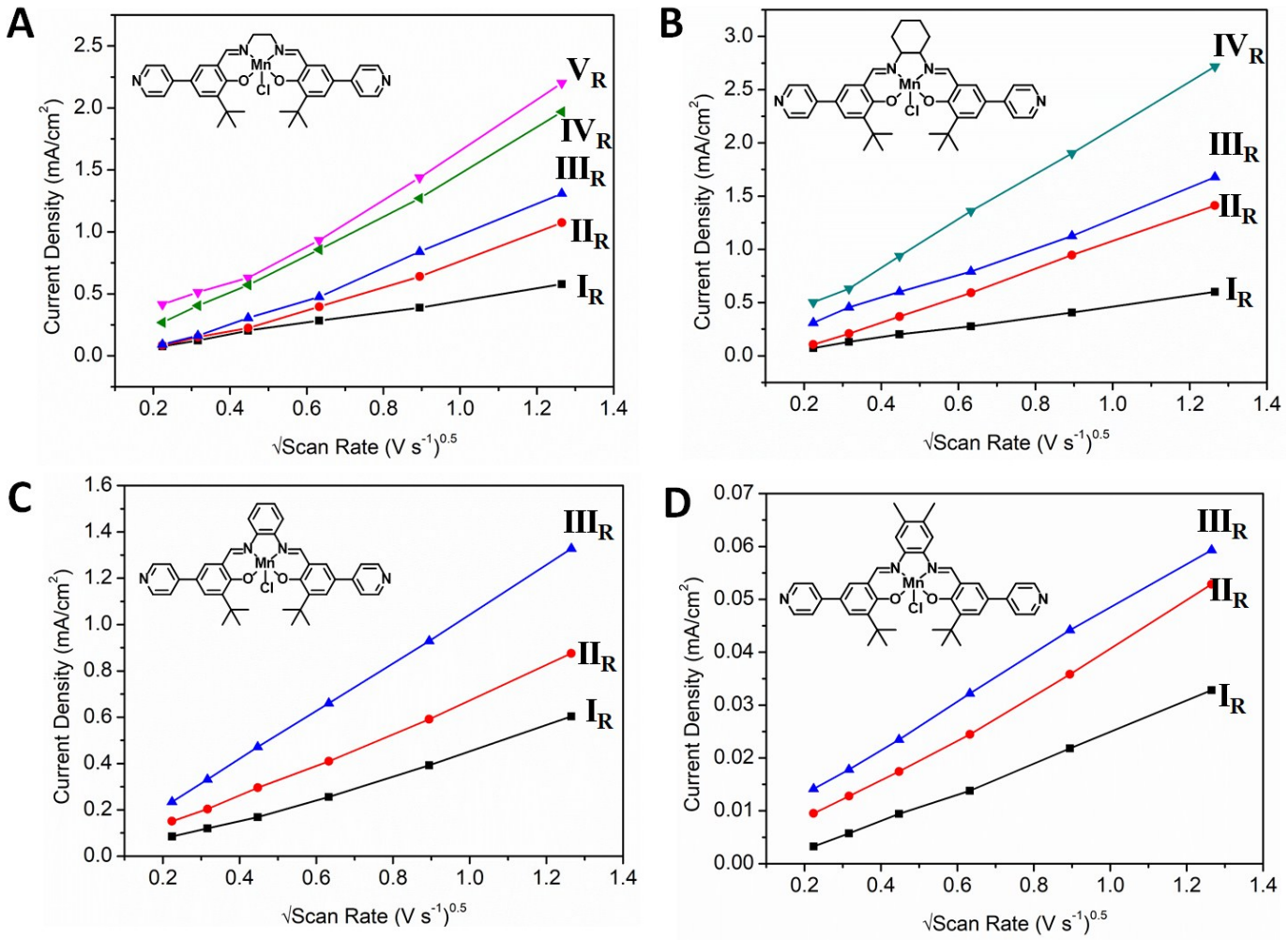

Figure S5. Scan rate dependence studies on each of the discrete salen complexes **A Mn^{t}P1Cl** (1 mM), **B Mn^{t}P2Cl** (1 mM), **C Mn^{t}P3Cl** (1 mM) and **D Mn^{t}P4Cl** (1 mM). (0.1 M $[(n\text{-}C_4H_9)_4N]PF_6$/DMF as the supporting electrolyte under N_2, Fc (1 mM) was used as an internal standard).

Spectroelectrochemistry

General: All salen metal complexes were soluble in DMF to undertake UV Vis NIR SEC. Only five of the eight metal complexes (**MnP1Cl, Mn^{t}P1Cl, Mn^{t}P2Cl, Mn^{t}P3Cl, Mn^{t}P4Cl**) were soluble in the reaction solution for IR SEC.

MnP1Cl: The first reduction process of **MnP1Cl** was ascribed to the Mn(III/II) reduction (Figure S6). Bands appeared at 18700 and 30380 cm^{-1}, accompanied by a decrease in the bands at 23930 and 33818 cm^{-1}. Interestingly, the bands in the electronic absorption spectrum for **MnP1Cl** are higher in energy than those in **Mn^{t}P1Cl**, indicating that the complexes without *tert*-butyl functional groups do not facilitate electronic communication as well as those with these functional groups. Furthermore, there is variability in the position of the isosbestic points at 21160, 24990 and 31730 cm^{-1}, consistent with a *quasi*-reversible process.

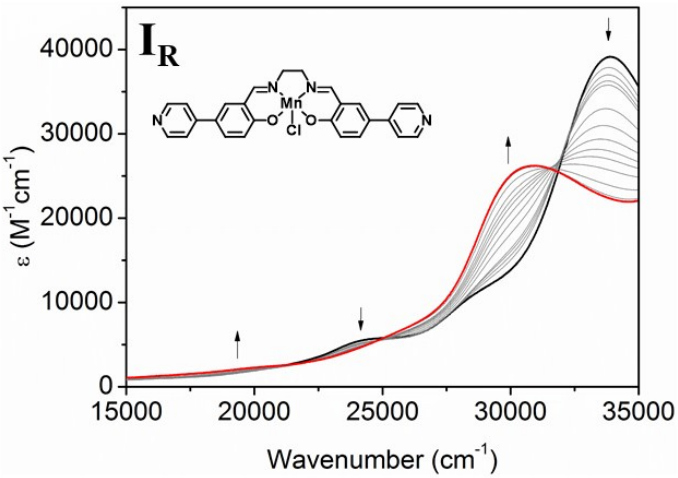

Figure S6. Solution state UV-Vis SEC of **A MnP1Cl** (0.23 mM) upon changing the potential from +0.1 V to –0.25 V vs. Ag/Ag$^+$(0.1 M [(n-C_4H_9)$_4$N]PF_6/DMF as the supporting electrolyte).

The second observed reduction in **MnP1Cl** is assigned to the imine. IR SEC of the II_R process at E_{pa} = –2.63 V *vs*. Fc^0/Fc^+ shows a minor shift in the $\nu_{C=N}$ stretch, outside of the error in the measurement (Figure S7A), which is smaller than that for **Mn^{t}P1Cl**. This shift may be attributed to the weaker dipole moment compared with the $\nu_{C=N}$ stretch.[8] The changes in the IR were consistent those in the UV-Vis, where the increase in the bands at 23760 and 29320 cm^{-1} was indicative of changes to the LMCT and n-π* transitions of the salen ligand (Figure S7C). There was a decrease in the band at 30970 cm^{-1}, with no discernible isosbestic point, suggestive of degradation.

The III_R process led to an unstable product across the aliphatic series of salens. For **MnP1Cl**, the immediate appearance of a broad signal at 1545 cm^{-1} suggests that degradation was occurring (Figure S7B).

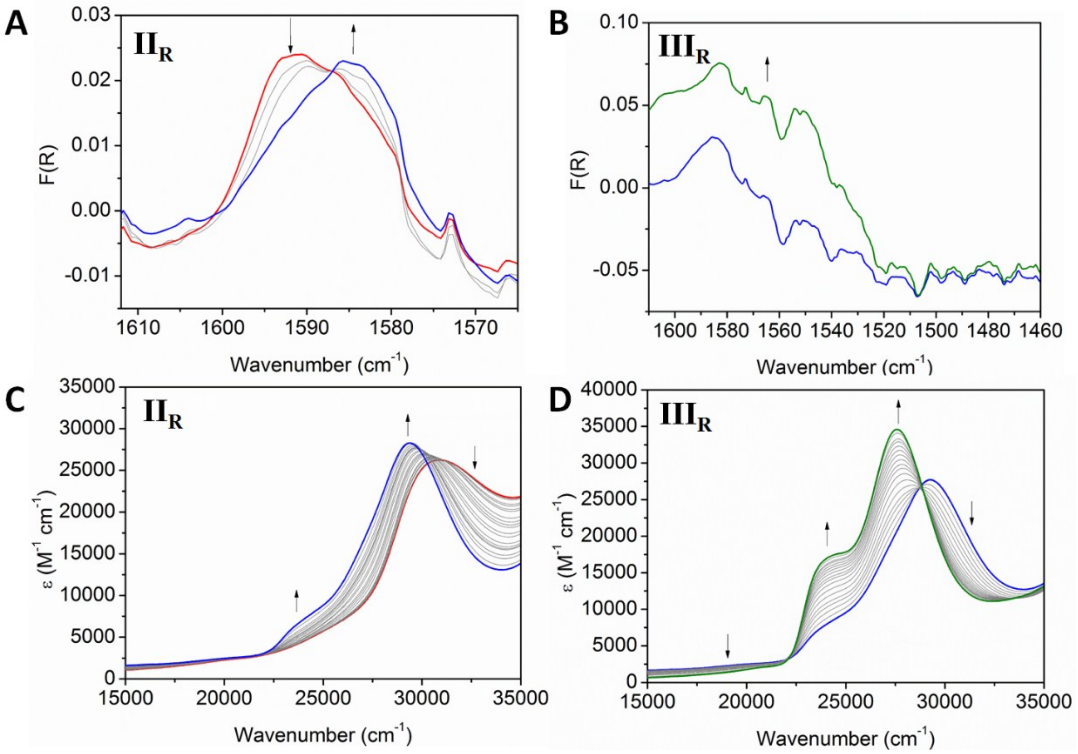

Figure S7. A Solution state IR SEC of **MnP1Cl** (4 mM) upon increasing the potential from **a)** −1.6 V to −1.8 V vs. Ag/Ag^+ and **B** holding at −1.8 V vs. Ag/Ag^+. Solution state UV-Vis SEC of **MnP1Cl** (0.23 mM) upon increasing the potential from **C** −1.6 V to −1.8 V vs. Ag/Ag^+ and **D** holding at −1.8 V vs. Ag/Ag^+. IR SEC was measured in 0.1 M $[(n\text{-}C_4H_9)_4N]PF_6$/MeCN/DMF (9:1) as the supporting electrolyte and UV-Vis SEC was measured in 0.1 M $[(n\text{-}C_4H_9)_4N]PF_6$/DMF as the supporting electrolyte.

Mn^{t}P2Cl: The I_R process for **Mn^{t}P2Cl** was examined at $E_{½}$ = –0.74 V *vs.* Fc^0/Fc^+ (Figure S8). New bands appeared at 19430, 26300, 29830 cm^{-1} and the band at 33220 cm^{-1} decreased. The UV-Vis spectrum for the salen core has been previously reported, with bands at 19880, 22940 and 26670 cm^{-1} having been assigned to the *d-d*, LMCT and n-π* electronic transitions, respectively.[7] In the present case, the growth in the *d-d* band and a change in the intensity of the MLCT band during reduction is consistent with a Mn(III/II) process. The *quasi*-reversible nature of the process is supported by the shift in the isosbestic point as the potential becomes more cathodic.

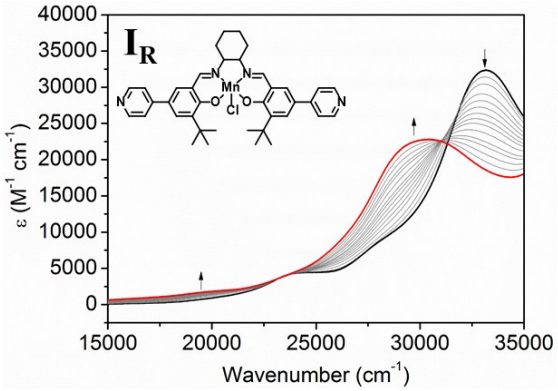

Figure S8. Solution state UV-Vis SEC of **B Mn^{t}P2Cl** (0.38 mM) upon changing the potential from +0.4 to –0.3 V vs. Ag/Ag^+(0.1 M $[(n\text{-}C_4H_9)_4N]PF_6$/DMF as the supporting electrolyte).

There is evidence for the assignment of the II_R process for **Mn^{t}P2Cl** as an imine reduction. Like **Mn^{t}P1Cl** and **MnPCl,** there was a shift in the imine stretch in the IR SEC (Figure S9A). The observed shift was larger than that observed in both **Mn^{t}P1Cl** and **MnP1Cl**. UV-Vis SEC reveals the growth of the MLCT and n-π* transitions (Figure S9C).

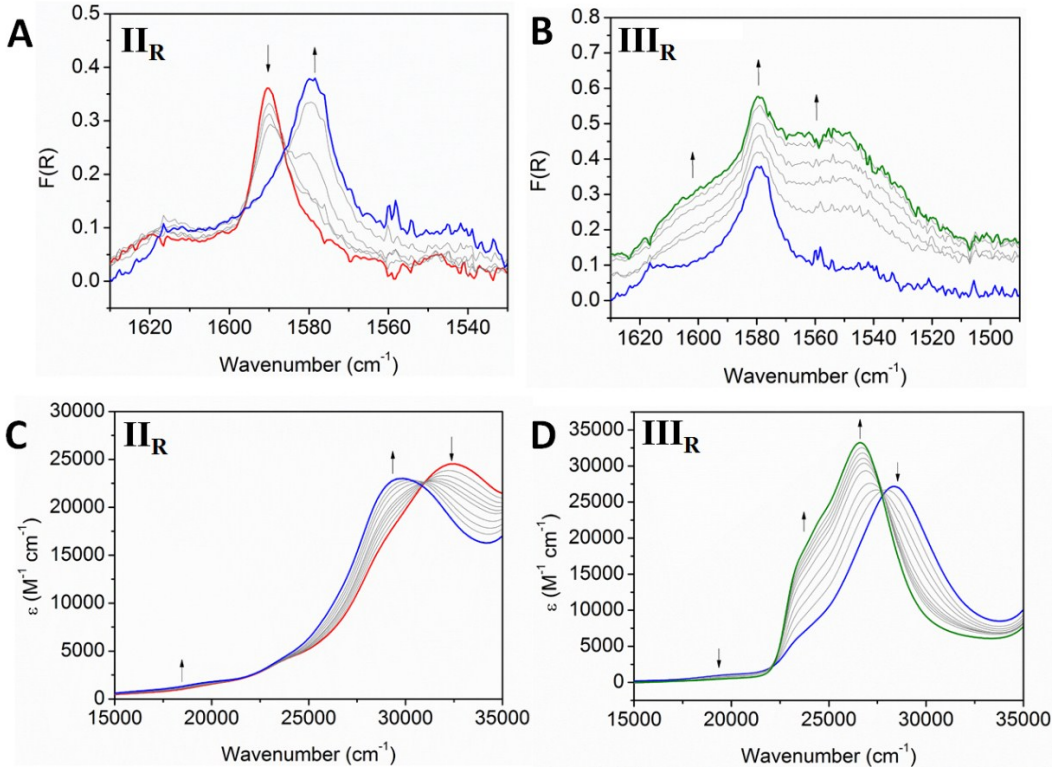

Figure S9. Solution state IR SEC of **Mn^{t}P2Cl** (4 mM) upon increasing the potential from **A** −1.5 to −2.0 V vs. Ag/Ag^+ and **B** −1.8 to −2.4 V vs. Ag/Ag^+. Solution state UV-Vis SEC (0.38 mM) increasing the potential from **C** −1.2 to −1.8 V vs. Ag/Ag^+ and **D** −1.9 to −2.4 V vs. Ag/Ag^+. IR SEC was measured on **Mn^{t}P2Cl** in 0.1 M $[(n\text{-}C_4H_9)_4N]PF_6$/MeCN/DMF (9:1) as the supporting electrolyte, while UV-Vis SEC was measured in 0.1 M $[(n\text{-}C_4H_9)_4N]PF_6$/DMF as the supporting electrolyte.

The III_R process in **Mn^{t}P2Cl** is ascribed to the generation of an asymmetric dianionic species similar to that observed in **Mn^{t}P1Cl.** IR SEC reveals the generation of bands at 1600 and 1550 cm^{-1}, with a preservation of $\nu_{C=N}$, consistent with generating an asymmetric dianionic species (Figure S9B). The UV-Vis SEC further suggests chemical instability of the reduced species, where the bands corresponding to the LMCT and n-π* transitions at 22940 and 26670 cm^{-1} increase dramatically upon reduction and the π-π* transitions disappear (Figure S9D). The shift in the isosbestic point from 31060 to 30720 cm^{-1} is indicative of multiple processes occurring in **Mn^{t}P2Cl.**

MnP2Cl: This complex was insoluble in the required solvent mixture for IR SEC; therefore, the measurement could not be undertaken. UV-Vis-NIR SEC was performed, whereby reduction processes similar to those found in **Mn^{t}P2Cl** could be observed (Figure S10). **MnP2Cl** exhibited similar features to **Mn^{t}P2Cl** with unstable isosbestic points, implying reduced stability.

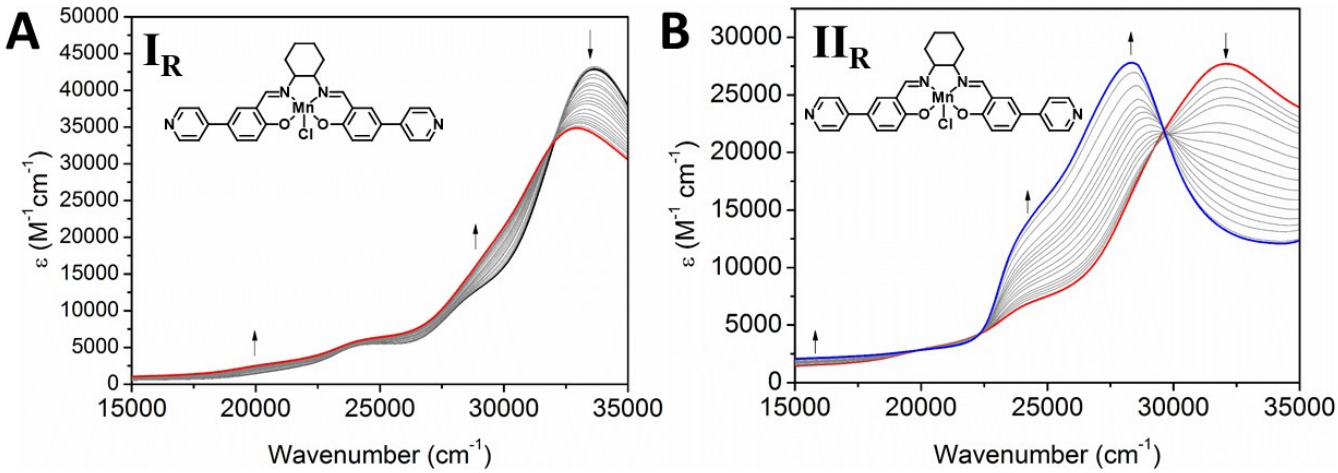

Figure S10. Solution state UV-Vis SEC of **MnP2Cl** (0.39 mM) upon increasing the potential from **A** 0 V to −0.3 V vs. Ag/Ag^+ and **B** from −1.4 V to −2.2 V vs. Ag/Ag^+ (0.1 M $[(n\text{-}C_4H_9)_4N]PF_6$/DMF as the supporting electrolyte).

MnP3Cl: This complex was also insoluble in the required solvent mixture for IR SEC; therefore, this measurement could not be undertaken. UV-Vis-NIR SEC was performed, whereby reduction processes like those found in **Mn^{t}P3Cl** could be observed (Figure S11). The absence of *tert*-butyl groups lowered the solubility of **MnP3Cl** and reduced the reversibility of the redox processes. UV-Vis SEC experiments performed on the I_R redox process revealed a decrease in the *d-d* band at 20300 cm^{-1} and increase in the LMCT transitions at 22170 and 24240 cm^{-1}. This is concurrent with the increase of the n-π* bands at 29940 cm^{-1} and the decrease of the π-π* bands at 33240 cm^{-1}.

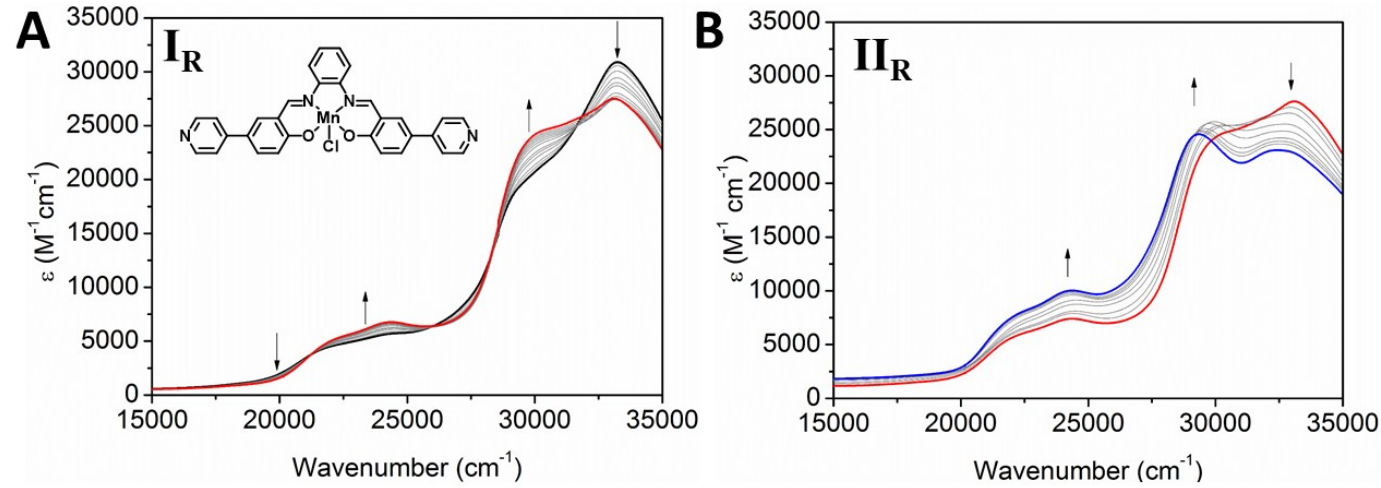

Figure S11. Solution state UV-Vis SEC of **MnP3Cl** (0.48 mM) upon increasing the potential from −0.1 V to −0.3 V vs. Ag/Ag^+ and **B** −1.2 V to −1.7 V vs. Ag/Ag^+. (0.1 M $[(n\text{-}C_4H_9)_4N]PF_6$/DMF as the supporting electrolyte)

Evidence for the degradation of **MnP3Cl** was observed during the II_R irreversible reduction process, suggesting that the presence of a *tert*-butyl substituent improves stability. For **MnP3Cl** there was a shift in the n-π* transitions from 30040 cm^{-1} upon application of the potential, which then red shifted to 29700 cm^{-1}. The shift of the band to lower energies is likely to indicate unstable reduced species since there were no clear isosbestic points.

Mn^{t}P4Cl: Experimentally, the reduction behaviour of **Mn^{t}P4Cl** was consistent with that observed for **Mn^{t}P3Cl**. The I_R redox process of **Mn^{t}P4Cl** at E_{pc} = –0.55 V *vs.* Fc^0/Fc^+ is related to the Mn(III/II) couple and is associated with the disappearance of the *d-d* transition at 20070 cm^{-1}, consistent with the change in the metal high spin d^4 to high spin d^5. The appearance of LMCT bands at 21810 and 23970 cm^{-1} indicates that the process is likely to be metal based. The challenge in reducing the electronically rich species manifested itself in the higher potentials required to facilitate the reduction.

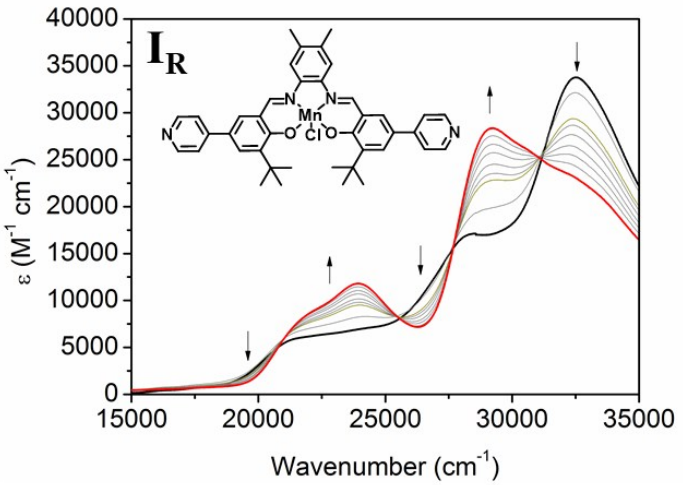

Figure S12. Solution state UV-Vis SEC of **Mn^{t}P4Cl** (0.36 mM) upon increasing the potential from +0.1 to –0.8 V vs. Ag/Ag^+ and UV-Vis SEC was measured in 0.1 M $[(n\text{-}C_4H_9)_4N]PF_6$/DMF as the supporting electrolyte.

UV-Vis SEC experiments were also performed on **Mn^{t}P4Cl.** Unlike the case of **Mn^{t}P3Cl**, the II_R redox process for **Mn^{t}P4Cl** at E_{pc} = –2.35 V *vs.* Fc^0/Fc^+ corresponded to only minor changes in the UV-Vis spectrum. IR SEC experiments revealed a loss of the imine functionality $\nu_{C=N}$ at 1584 cm^{-1}, consistent with the delocalisation of charge across the aromatic bridging moiety. The growth of a broad band at 1555 cm^{-1}, consistent with the generation of the radical anion on the pyridyl group, subsequently occurs.

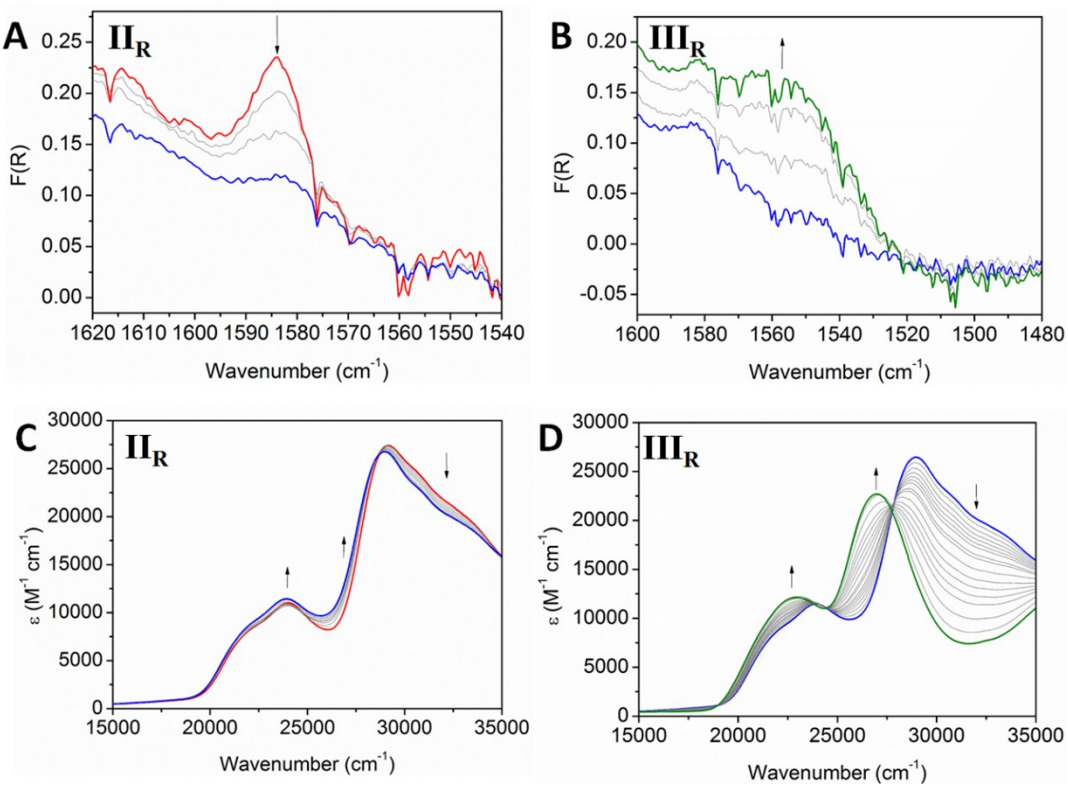

Figure S13. Solution state IR SEC of **Mn^{t}P4Cl** (4 mM) upon increasing the potential from **a)** –1.6 to –1.9 V vs. Ag/Ag^+ and **b)** –2.0 to –2.2 V vs. Ag/Ag^+. Solution state UV-Vis SEC of **Mn^{t}P4Cl** (0.36 mM) upon increasing the potential from **c)** –1.6 to –1.9 V vs. Ag/Ag^+ and **d)** –2.0 to –2.2 V vs. Ag/Ag^+. IR SEC was measured in 0.1 M $[(n\text{-}C_4H_9)_4N]PF_6$/MeCN/DMF (9:1) as the supporting electrolyte, while UV-Vis SEC was measured in 0.1 M $[(n\text{-}C_4H_9)_4N]PF_6$/DMF as the supporting electrolyte.

MnP4Cl: This complex was insoluble in the required solvent mixture for IR SEC; therefore, this measurement could not be undertaken. UV-Vis-NIR SEC were performed where possible on **MnP4Cl**. The first process is consistent with a Mn(III/II) reduction. There were noticeable increases in the bands at 22170, 24500 and 30070 cm^{-1} and decreases in bands at 27100 and 33240 cm^{-1}.

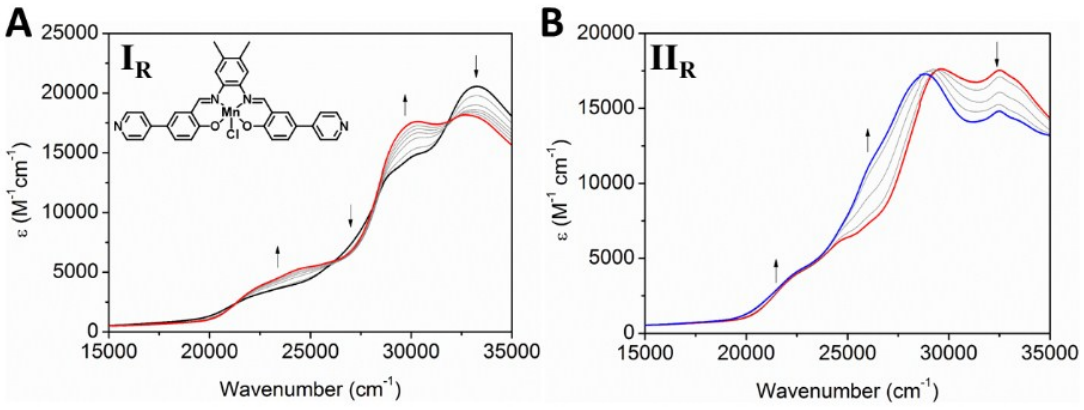

Figure S14. A Solution state UV-Vis SEC of **MnP4Cl** (0.41 mM) upon increasing the potential from +0.2 V to –0.1 V vs. Ag/Ag^+ and **D** –0.9 V to –1.3 V vs. Ag/Ag^+ (0.1 M $[(n\text{-}C_4H_9)_4N]PF_6$/DMF as the supporting electrolyte).

Evidence for the degradation of **MnP4Cl** was observed during the II_R irreversible reduction process, suggesting that the presence of a *tert*-butyl substituent improves stability. The UV-Vis SEC for this process shows the appearance of bands at 20260, 24630, 26000 and 29000 cm^{-1}, with a decrease in bands at 29640 and 32540 cm^{-1}. The absence of an isosbestic point during the second reduction process indicates that more than one species is formed in solution.

Computational Study

The preliminary investigation used two simpler models to gauge the likely spin state and coordination environment. These computations were carried out at the B-PW91/6-31+G(d) level with the incorporation of a solvent (DMF) continuum (SMD). The models employed are:

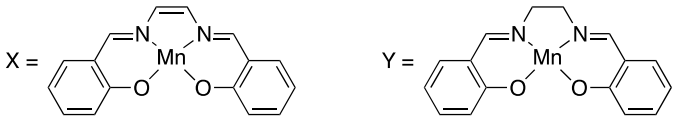

Table S1. The relative energies of various model salen complexes at different redox states. Energies are shown in kJ mol^{-1}.

	Model spin state	No axial ligand	Cl^-	DMF	Cl^- and DMF
X^+					
	singlet	0.0	-176.2	-154.9	-195.9
	triplet	-295.6	-395.1	-371.9	-434.2
	quintet	-396.5	-447.6	-429.6	-442.7
X^0					
	doublet	0.0	-17.9	-20.5	-29.6
	quartet	-89.8	-87.0	-93.1	-25.0
	sextet	-66.7	-97.6	-87.5	-98.3
X^-					
	singlet	0.0	32.8	3.8	49.6
	triplet	-143.5	-39.3	-52.6	-22.7
	quintet	-135.5	-113.4	-128.0	-131.9
X^{2-}					
	doublet	0.0	103.8	81.6	125.5
	quartet	-15.9	-15.3	-1.8	-15.5
	sextet	51.9	31.4	20.1	27.4
Y^+					
	singlet	0.0	-142.0	-101.3	-159.8
	triplet	-144.0	-222.7	-202.4	-261.3
	quintet	-232.1	-276.4	-259.8	-267.9
Y^0					
	doublet	0.0	-8.5	-12.2	-5.7
	quartet	-88.0	-82.2	-88.7	-88.8
	sextet	-40.1	-62.4	-54.0	-62.9
Y^-					
	singlet	0.0	51.1	22.4	48.6
	triplet	-84.4	-89.6	-73.6	-88.3
	quintet	-63.4	-44.2	-57.2	-61.3
Y^{2-}					
	doublet	0.0	4.6	-1.0	4.9
	quartet	20.3	24.1	19.7	24.2
	sextet	37.9	38.7	36.9	41.2

The models demonstrate that the high-spin state is preferred over the low-spin ones for the more positively charge redox levels, but the intermediate spin states become increasingly favourable as the complex becomes more negatively charged. It can also be seen that as the species becomes more negatively charged, the coordination with Cl^- and DMF ligands also becomes less favourable. These results can be qualitatively rationalised from the point of view of a combination of standard crystal field theory and the 18-electron rule. When comparing X and Y, it is observed that the presence of the unsaturated linkage in X leads to a stronger preference for higher spin states.

For a more limited set of species for the ^{t}P1 and ^{t}P3 systems, we have also performed similar calculations and at the higher B3-PW91/6-311+G(3df,2p) level to further validate the above findings. The results, which are consistent with those for the smaller model, have been included and discussed in the main text. Finally, we give in this supporting information the optimised geometries for the complexes shown in the main text.

[Mn(^{t}P1)(Cl)(DMF)]^0

Mn	-0.051157	-1.008684	-0.296835
Cl	-0.393393	-0.996614	-2.616103
O	-1.444432	0.277382	-0.060794
O	1.354695	0.281749	-0.430379
N	1.226952	-2.457529	-0.470090
N	-1.322873	-2.456270	-0.070119
N	-9.951552	-0.485460	-0.271831
N	9.855209	-0.481633	-0.135019
C	-2.754493	0.161948	-0.123039
C	-4.796207	-1.258425	-0.160654
H	-5.227335	-2.264044	-0.130956
C	2.664661	0.159748	-0.447740
C	-7.096255	-0.249816	-0.222301
C	-3.385763	-1.138706	-0.126665
C	-4.984878	1.144882	-0.190637
H	-5.630307	2.022647	-0.243943
C	4.703195	-1.263310	-0.367807
H	5.130956	-2.269352	-0.312134
C	-3.601349	1.338969	-0.160941
C	3.292811	-1.142256	-0.410967
C	-5.619398	-0.131277	-0.193390
C	2.533870	-2.363381	-0.456536
H	3.110307	-3.298582	-0.509093
C	-2.629074	-2.359235	-0.043291
H	-3.205266	-3.290487	0.059076
C	7.003142	-0.254149	-0.287575
C	-7.747376	-1.360394	-0.811094
H	-7.175007	-2.158198	-1.291859
H	1.279464	-4.585135	-0.336503
C	-7.940333	0.738443	0.338420
H	-7.524935	1.619894	0.833858
C	2.929537	2.751165	-0.718933
C	7.803642	0.742818	0.319641
H	7.352049	1.628224	0.774833
C	5.527818	-0.137029	-0.362804
C	-9.329979	0.577487	0.287897
H	-9.983144	1.340482	0.726845
C	-3.005909	2.765991	-0.181659
C	3.515498	1.332869	-0.522269
C	4.897420	1.138403	-0.453303
H	5.547619	2.012516	-0.510559
H	-1.373279	-4.584233	-0.183678
C	-9.144886	-1.430726	-0.807456
H	-9.648665	-2.288488	-1.267674
C	2.120672	2.793311	-2.042685
H	1.299369	2.062664	-2.038668
H	1.688946	3.799352	-2.188461
H	2.773502	2.577266	-2.906817
C	2.013549	3.134975	0.470874
H	1.151210	2.459720	0.548310
H	2.570840	3.104391	1.423620
H	1.633191	4.162823	0.334743
C	-4.094587	3.861986	-0.247248
H	-3.602650	4.849653	-0.261583
H	-4.710854	3.789089	-1.160079
H	-4.766292	3.842367	0.628435
C	-2.186862	3.012799	1.112195
H	-1.362627	2.293387	1.212359
H	-1.758426	4.030589	1.098648
H	-2.831289	2.929340	2.005286
C	9.193845	0.585546	0.368126
H	9.813129	1.355173	0.843115
C	0.603584	-3.776785	-0.660041
H	0.389941	-3.900196	-1.736092
C	-2.101852	2.941834	-1.429396
H	-1.282638	2.210188	-1.443829
H	-2.689585	2.821563	-2.356595
H	-1.663723	3.955565	-1.436696
C	7.696011	-1.369557	-0.816553
H	7.160579	-2.174415	-1.327158
C	9.090057	-1.435293	-0.714943
H	9.626779	-2.296477	-1.129301
C	-0.697128	-3.773811	0.134096
H	-0.484689	-3.893636	1.210536
C	4.028914	3.834221	-0.816641
H	3.547921	4.814949	-0.972726
H	4.631301	3.906313	0.105529
H	4.713055	3.664557	-1.665861
O	0.244503	-1.115807	1.736077
C	0.384173	-0.089855	2.471923
N	0.556280	-0.151786	3.795720
C	0.717191	1.066829	4.592358
H	-0.088468	1.129176	5.342050
H	1.688796	1.044937	5.112224
H	0.674905	1.948620	3.938797
C	0.597716	-1.422868	4.520443
H	1.572099	-1.527313	5.025084
H	-0.200673	-1.438163	5.280240
H	0.455473	-2.252379	3.817945
H	0.372905	0.923222	2.047093

[Mn(^{t}P1)(Cl)]$^{-1}$

Mn	-0.003667	-1.061962	0.099636
Cl	0.265661	-1.349308	2.747195
O	1.387490	0.246231	-0.039791
O	-1.424349	0.228891	0.130754
N	-1.296371	-2.494897	-0.038896
N	1.249037	-2.459799	-0.395156
N	9.893835	-0.484996	-0.510849
N	-9.913979	-0.472949	-0.600439
C	2.699536	0.138022	-0.119679
C	4.737094	-1.256740	-0.409793

H	5.167453	-2.246498	-0.594039
C	-2.734582	0.121848	0.021049
C	7.037503	-0.251105	-0.366899
C	3.326150	-1.151310	-0.329250
C	4.931662	1.129329	-0.104428
H	5.576225	2.002010	0.008828
C	-4.777420	-1.280317	-0.185006
H	-5.212529	-2.280605	-0.280305
C	3.546788	1.308359	-0.018308
C	-3.367988	-1.177208	-0.077602
C	5.562745	-0.135096	-0.292859
C	-2.613769	-2.399660	-0.095069
H	-3.188660	-3.334037	-0.170429
C	2.561557	-2.352575	-0.516994
H	3.122763	-3.255430	-0.798989
C	-7.065169	-0.255376	-0.340662
C	7.717693	-1.429758	0.027234
H	7.170314	-2.287549	0.427161
H	-1.366928	-4.588110	-0.460135
C	7.856842	0.805552	-0.834215
H	7.421561	1.745955	-1.181893
C	-2.968942	2.719816	0.123885
C	-7.843775	0.753541	-0.958703
H	-7.375906	1.645450	-1.383506
C	-5.593754	-0.146165	-0.211763
C	9.246071	0.642726	-0.883789
H	9.877118	1.460755	-1.250317
C	2.947675	2.718666	0.191251
C	-3.574179	1.301979	0.002340
C	-4.956895	1.125766	-0.117392
H	-5.597284	2.008903	-0.106389
H	1.295879	-4.591695	-0.512458
C	9.112015	-1.496115	-0.065150
H	9.635811	-2.408052	0.244206
C	-2.195709	2.853067	1.462472
H	-1.384796	2.115389	1.537177
H	-1.756632	3.863247	1.546191
H	-2.875761	2.709426	2.321000
C	-2.018403	2.983913	-1.073211
H	-1.205648	2.245572	-1.111649
H	-2.572860	2.941995	-2.027765
H	-1.570972	3.990010	-0.987146
C	4.032006	3.816714	0.288261
H	3.538079	4.793206	0.432008
H	4.711219	3.662784	1.144732
H	4.641866	3.888564	-0.628987
C	2.037368	3.077915	-1.012534
H	1.222288	2.350573	-1.131194
H	1.592657	4.078321	-0.866408
H	2.621840	3.102261	-1.949638
C	-9.231347	0.601018	-1.059909
H	-9.830962	1.380790	-1.543758
C	-0.694059	-3.838775	-0.008764
H	-0.514323	-4.114654	1.045402
C	2.132785	2.760511	1.510459
H	1.317241	2.024442	1.505039
H	2.783917	2.549979	2.377483
H	1.696051	3.765098	1.653134
C	-7.781705	-1.377366	0.143483
H	-7.267869	-2.192967	0.659232
C	-9.170983	-1.438093	-0.010011
H	-9.723606	-2.305526	0.369230
C	0.628063	-3.748794	-0.760115
H	0.445428	-3.758708	-1.850262
C	-4.045611	3.829374	0.106478
H	-3.547613	4.810117	0.197340
H	-4.624038	3.840518	-0.833589
H	-4.754264	3.741259	0.948317

[Mn(^{t}P1)]$^{-1}$

Mn	-0.000036	-1.132467	0.001324
O	-1.401967	0.162408	-0.153098
O	1.402017	0.162351	0.154922
N	1.248620	-2.523140	-0.269199
N	-1.248872	-2.522945	0.272004
N	-9.925740	-0.524472	0.230463
N	9.925455	-0.524664	-0.235398
C	-2.723781	0.054014	-0.099768
C	-4.766033	-1.325134	0.191469
H	-5.209541	-2.314813	0.344953
C	2.723798	0.053922	0.100760
C	-7.061838	-0.309216	0.091586
C	-3.349776	-1.239603	0.127111
C	-4.956160	1.049366	-0.227692
H	-5.591753	1.928684	-0.338666
C	4.765822	-1.325216	-0.192171
H	5.209237	-2.314875	-0.346103
C	-3.561744	1.212457	-0.288936
C	3.349616	-1.239704	-0.126597
C	-5.587879	-0.201951	0.019389
C	2.591460	-2.447934	-0.268447
H	3.153515	-3.382210	-0.406450
C	-2.591714	-2.447804	0.269753
H	-3.153873	-3.382091	0.407267
C	7.061679	-0.309337	-0.094020
C	-7.709716	-1.327137	0.837281
H	-7.132654	-2.057190	1.411022
H	1.332407	-4.655263	-0.110122
C	-7.922452	0.596257	-0.579314
H	-7.519451	1.400962	-1.199615
C	2.947784	2.609425	0.552393
C	7.922889	0.595866	0.576475
H	7.520473	1.400371	1.197418
C	5.587799	-0.202043	-0.020648
C	-9.310248	0.450446	-0.479429
H	-9.969941	1.151025	-1.004840
C	-2.947359	2.609591	-0.551052
C	3.561923	1.212320	0.289525
C	4.956291	1.049230	0.227167
H	5.591991	1.928523	0.337785
H	-1.332745	-4.655161	0.114086
C	-9.106446	-1.391291	0.871436
H	-9.600861	-2.178047	1.453358
C	2.052722	3.029832	-0.642657
H	1.239794	2.309079	-0.807008
H	1.606237	4.022820	-0.454004
H	2.648838	3.100099	-1.570242
C	2.111339	2.578122	1.859536
H	1.306810	1.830958	1.803192
H	2.751906	2.334514	2.726160
H	1.656749	3.567995	2.045276
C	-4.020898	3.709283	-0.725042
H	-3.517917	4.673613	-0.914201
H	-4.689019	3.513388	-1.581660
H	-4.644155	3.835463	0.177314
C	-2.052913	3.029595	0.644605
H	-1.240136	2.308735	0.809224
H	-1.606254	4.022599	0.456456
H	-2.649534	3.099668	1.571882
C	9.310596	0.450028	0.475362
H	9.970759	1.150397	1.000463
C	0.635468	-3.857573	-0.424192
H	0.378453	-4.024098	-1.486963
C	-2.110201	2.578575	-1.857743
H	-1.305833	1.831251	-1.801189
H	-2.750334	2.335349	-2.724794
H	-1.655334	3.568427	-2.042920
C	7.708882	-1.327044	-0.840581
H	7.131283	-2.056869	-1.414070
C	9.105583	-1.391247	-0.875950
H	9.599460	-2.177826	-1.458568
C	-0.635782	-3.857317	0.427693
H	-0.378744	-4.023255	1.490547
C	4.021512	3.708970	0.726129
H	3.518713	4.673295	0.915801
H	4.690044	3.512777	1.582357
H	4.644329	3.835346	-0.176504

[Mn(^{t}P1)]$^{-2}$

Mn	-0.002225	-1.125059	0.005779
O	1.399154	0.150607	0.186485
O	-1.403017	0.155678	-0.154420
N	-1.245265	-2.521591	0.280873
N	1.239410	-2.517941	-0.297962
N	9.983141	-0.501402	-0.295832
N	-9.976305	-0.504516	0.212201
C	2.722517	0.040651	0.119881
C	4.772814	-1.328621	-0.202481
H	5.198344	-2.317687	-0.398464
C	-2.726581	0.045164	-0.103334
C	7.075676	-0.293897	-0.112608
C	3.350697	-1.243495	-0.127456
C	4.957142	1.039474	0.236196
H	5.577320	1.923304	0.383667
C	-4.777758	-1.330268	0.177050
H	-5.212901	-2.323616	0.329098
C	3.566292	1.198033	0.319637
C	-3.355462	-1.244347	0.121797
C	5.611990	-0.204655	-0.028477
C	-2.592266	-2.447486	0.267520
H	-3.151175	-3.384926	0.402067
C	2.585975	-2.444380	-0.286337
H	3.143918	-3.380078	-0.436646
C	-7.075915	-0.295459	0.073417
C	7.763189	-1.530312	-0.367033
H	7.214515	-2.465433	-0.505727
H	-1.341021	-4.648376	0.076234
C	7.952427	0.827220	0.044047
H	7.562337	1.829522	0.240174
C	-2.948717	2.601932	-0.555796
C	-7.952726	0.730386	-0.398025
H	-7.558800	1.641236	-0.857703
C	-5.610657	-0.204634	0.002489
C	9.334719	0.679843	-0.051485
H	9.979816	1.558796	0.072940
C	2.952407	2.586544	0.628443
C	-3.566950	1.205775	-0.294417
C	-4.959657	1.044778	-0.236701
H	-5.584381	1.931099	-0.351096
H	1.333751	-4.647722	-0.126506
C	9.153700	-1.573261	-0.445294
H	9.649831	-2.532868	-0.641721
C	-2.058486	3.022230	0.643260
H	-1.250442	2.297249	0.813588
H	-1.605997	4.013013	0.455982
H	-2.659803	3.096903	1.567305
C	-2.104204	2.568448	-1.857899
H	-1.303821	1.817152	-1.796017
H	-2.740567	2.327168	-2.728460
H	-1.643967	3.556344	-2.041851
C	4.022733	3.686201	0.822519
H	3.517508	4.642969	1.042853
H	4.699941	3.470318	1.667259
H	4.637371	3.840248	-0.081471
C	2.043530	3.038174	-0.545009
H	1.232973	2.317609	-0.721764
H	1.594096	4.023492	-0.324438
H	2.630203	3.137593	-1.476134
C	-9.336522	0.585093	-0.310952
H	-9.988106	1.383682	-0.687225
C	-0.639346	-3.860218	0.407672
H	-0.382374	-4.055243	1.465953
C	2.127906	2.518518	1.941955
H	1.326225	1.769186	1.872633
H	2.777326	2.254363	2.796069
H	1.670769	3.501143	2.159042
C	-7.751949	-1.436946	0.617433
H	-7.190338	-2.280001	1.029165
C	-9.144398	-1.485388	0.662637
H	-9.638170	-2.366384	1.092752
C	0.632469	-3.854037	-0.445393
H	0.375137	-4.032177	-1.506545
C	-4.016928	3.705786	-0.737225
H	-3.509478	4.668084	-0.926039
H	-4.681824	3.510708	-1.596635
H	-4.644522	3.836580	0.161512

[Mn(^{t}P3)(Cl)(DMF)]^0

Mn	0.029758	0.682727	-0.228484
Cl	0.096230	0.622188	-2.559149
O	1.405597	-0.623448	-0.083333
O	-1.353398	-0.625837	-0.203087
N	-1.264032	2.145881	-0.255551
N	1.326070	2.142584	-0.223053
N	9.903998	-0.037240	-0.624289
N	-9.860482	0.004000	-0.423256
C	2.713111	-0.532093	-0.151956
C	4.776043	0.847339	-0.341408
H	5.224389	1.840245	-0.446188
C	-2.659350	-0.527061	-0.315227
C	7.052879	-0.206879	-0.424394
C	3.360254	0.756977	-0.262531
C	4.922737	-1.555569	-0.199103
H	5.556322	-2.442425	-0.153078
C	-4.720754	0.865423	-0.348691
H	-5.169596	1.862773	-0.309522
C	3.540397	-1.722010	-0.098648
C	-3.303782	0.767589	-0.312522
C	5.575980	-0.293013	-0.323131
C	-2.578874	1.999484	-0.268408
H	-3.198410	2.902555	-0.255932
C	2.639219	1.991219	-0.274968
H	3.259913	2.892132	-0.326922
C	-7.003221	-0.179183	-0.409812
C	7.774798	0.898016	0.086012
H	7.262639	1.716354	0.599118
C	-1.373539	4.663650	-0.240962
H	-2.464041	4.691978	-0.264348
C	7.821915	-1.223742	-1.037804
H	7.345201	-2.102326	-1.480204
C	-2.864111	-3.123070	-0.577947
C	-7.820505	-1.186083	0.156059
H	-7.382130	-2.062158	0.641257
C	-5.523326	-0.272298	-0.398090
C	9.214129	-1.094123	-1.110097
H	9.810333	-1.878477	-1.590309
C	2.924027	-3.128779	0.073756
C	-3.483861	-1.713817	-0.431237
C	-4.869147	-1.539272	-0.449122
H	-5.501656	-2.422879	-0.543444
C	1.442874	4.659670	-0.181930
H	2.533440	4.684390	-0.151828
C	9.168225	0.935417	-0.038512
H	9.728906	1.788329	0.360835
C	-1.984347	-3.162266	-1.855568
H	-1.187643	-2.405721	-1.823795
H	-1.515814	-4.156626	-1.960236
H	-2.597639	-2.981088	-2.755876
C	-2.010795	-3.477433	0.666816
H	-1.164813	-2.787843	0.787836
H	-2.622725	-3.447585	1.585508
H	-1.606701	-4.499906	0.563799
C	3.996041	-4.242023	0.113762
H	3.492019	-5.215435	0.240011
H	4.582494	-4.294039	-0.819727
H	4.696773	-4.122149	0.958149
C	2.142078	-3.196810	1.412213
H	1.335400	-2.451597	1.451513
H	1.694097	-4.198525	1.535699
H	2.818102	-3.021418	2.267762
C	-9.213609	-1.050122	0.123706
H	-9.847532	-1.826797	0.566706
C	-0.675528	3.439193	-0.235636
C	1.980741	-3.440911	-1.116893
H	1.170976	-2.703507	-1.197576

H	2.542098	-3.444705	-2.067958
H	1.529871	-4.440430	-0.986791
C	-7.680045	0.922531	-0.984631
H	-7.127530	1.732772	-1.467807
C	-9.078643	0.966832	-0.963942
H	-9.603980	1.817083	-1.413720
C	0.738827	5.870804	-0.183524
H	1.292356	6.813623	-0.158332
C	0.741625	3.437181	-0.213536
C	-3.937908	-4.226163	-0.723622
H	-3.431965	-5.199596	-0.841106
H	-4.589495	-4.298690	0.164423
H	-4.575840	-4.078384	-1.612010
C	-0.666602	5.872847	-0.215554
H	-1.217988	6.817246	-0.218258
O	0.010116	0.838933	1.818491
C	-0.384338	-0.080978	2.601546
N	-0.337122	0.019443	3.932761
C	-0.824257	-1.065320	4.787988
H	-0.005601	-1.427416	5.430858
H	-1.643573	-0.695408	5.425775
H	-1.192562	-1.893066	4.166964
C	0.189592	1.206261	4.609090
H	-0.597448	1.648185	5.241667
H	1.040113	0.917181	5.247724
H	0.519625	1.939591	3.863859
H	-0.801479	-1.019964	2.211017

[Mn(^{t}P3)(Cl)]$^{-1}$

Mn	-0.000378	0.698779	0.171192
Cl	-0.025468	0.872219	2.797518
O	-1.383534	-0.618461	0.020974
O	1.386222	-0.616398	0.074908
N	1.288899	2.143029	-0.076867
N	-1.287983	2.144540	-0.079384
N	-9.895106	0.002293	-0.393770
N	9.885639	0.002190	-0.532368
C	-2.692986	-0.523779	-0.074285
C	-4.753791	0.863838	-0.221000
H	-5.202995	1.861799	-0.243614
C	2.696345	-0.523145	-0.013231
C	-7.036163	-0.180674	-0.287773
C	-3.337301	0.772625	-0.140151
C	-4.906624	-1.543794	-0.184665
H	-5.537485	-2.432579	-0.227692
C	4.753890	0.860422	-0.226869
H	5.200223	1.854174	-0.335722
C	-3.520445	-1.711932	-0.126215
C	3.338364	0.771022	-0.128181
C	-5.558167	-0.275029	-0.229996
C	2.611005	1.999041	-0.178779
H	3.218887	2.897375	-0.328537
C	-2.611573	2.002791	-0.158488
H	-3.222746	2.904293	-0.270936
C	7.033350	-0.184652	-0.324993
C	-7.696754	0.903042	-0.915420
H	-7.130979	1.699830	-1.405527
C	1.411202	4.663077	-0.173764
H	2.502136	4.689030	-0.154869
C	-7.873681	-1.169145	0.282843
H	-7.452044	-2.030233	0.807911
C	2.910557	-3.122026	0.132480
C	7.809288	-1.198592	-0.936244
H	7.337853	-2.082226	-1.374272
C	5.558014	-0.278494	-0.219925
C	-9.264778	-1.034619	0.203870
H	-9.912070	-1.798036	0.650812
C	-2.897403	-3.126769	-0.133130
C	3.526168	-1.710663	-0.004585
C	4.909880	-1.544996	-0.110391
H	5.544780	-2.431448	-0.076883
C	-1.406475	4.665038	-0.187213
H	-2.497410	4.693133	-0.182881
C	-9.095003	0.948240	-0.938402
H	-9.605115	1.785384	-1.428719
C	2.124458	-3.229091	1.465778
H	1.321154	-2.481885	1.525025
H	1.673560	-4.233108	1.558046
H	2.798928	-3.081985	2.327998
C	1.970308	-3.397361	-1.069759
H	1.159865	-2.657872	-1.124528
H	2.533311	-3.368650	-2.019733
H	1.519802	-4.401109	-0.974809
C	-3.963360	-4.245190	-0.192149
H	-3.451861	-5.223089	-0.195234
H	-4.637917	-4.229908	0.681449
H	-4.578663	-4.194134	-1.107184
C	-1.996724	-3.285064	-1.386305
H	-1.193753	-2.535138	-1.404718
H	-1.535061	-4.288113	-1.397002
H	-2.593204	-3.178518	-2.309868
C	9.200298	-1.060793	-1.012102
H	9.800086	-1.843593	-1.490635
C	0.710351	3.442020	-0.135757
C	-2.069328	-3.352195	1.159038
H	-1.263942	-2.612116	1.259543
H	-2.715588	-3.285051	2.052268
H	-1.617330	-4.359876	1.145381
C	7.751563	0.926034	0.179981
H	7.236229	1.742551	0.692820
C	9.144205	0.971935	0.051835
H	9.700167	1.829771	0.447459
C	-0.698042	5.878170	-0.226908
H	-1.250998	6.821596	-0.255794
C	-0.708065	3.443076	-0.138834
C	3.980595	-4.238012	0.141512
H	3.475205	-5.213956	0.241680
H	4.567473	-4.266272	-0.792920
H	4.681691	-4.142328	0.988762
C	0.705001	5.877249	-0.219174
H	1.259497	6.819969	-0.240888

[Mn(^{t}P3)]$^{-1}$

Mn	-0.000000	0.783147	0.000141
O	1.370031	-0.523522	-0.122080
O	-1.370037	-0.523505	0.122404
N	-1.296255	2.228794	-0.036955
N	1.296270	2.228792	0.037159
N	9.900732	-0.075830	0.244291
N	-9.900694	-0.075827	-0.245215
C	2.698043	-0.450991	-0.116214
C	4.773963	0.876684	0.141217
H	5.248405	1.855615	0.266985
C	-2.698047	-0.450967	0.116364
C	7.036309	-0.209010	0.089262
C	3.351953	0.833358	0.060346
C	4.894661	-1.513710	-0.215618
H	5.506099	-2.412026	-0.306376
C	-4.773933	0.876686	-0.141460
H	-5.248361	1.855607	-0.267381
C	3.495903	-1.637471	-0.278408
C	-3.351936	0.833372	-0.060373
C	5.558617	-0.274586	0.008778
C	-2.643305	2.066936	-0.139745
H	-3.255360	2.962634	-0.284994
C	2.643332	2.066923	0.139772
H	3.255413	2.962618	0.284933
C	-7.036277	-0.209002	-0.089732
C	7.706002	0.787951	0.841677
H	7.144793	1.531858	1.413426
C	-1.410176	4.741427	-0.018906
H	-2.502236	4.767559	-0.021940
C	7.872050	-1.136698	-0.580347
H	7.447894	-1.927309	-1.204667
C	-2.841556	-3.020563	0.513477
C	-7.872132	-1.136623	0.579829

H	-7.448097	-1.927190	1.204291
C	-5.558608	-0.274570	-0.009019
C	9.263225	-1.030637	-0.472480
H	9.906124	-1.747644	-0.996385
C	2.841501	-3.020629	-0.513098
C	-3.495933	-1.637429	0.278568
C	-4.894682	-1.513669	0.215603
H	-5.506133	-2.411974	0.306403
C	1.410186	4.741430	0.019312
H	2.502245	4.767575	0.022355
C	9.104125	0.812290	0.883871
H	9.617967	1.582618	1.470744
C	-1.948012	-3.397897	-0.696532
H	-1.155805	-2.654167	-0.857381
H	-1.475212	-4.382092	-0.529070
H	-2.552015	-3.467790	-1.619024
C	-1.995516	-2.984330	1.814275
H	-1.212208	-2.214701	1.765121
H	-2.636088	-2.771894	2.688950
H	-1.511522	-3.963197	1.981598
C	3.883764	-4.150816	-0.681233
H	3.353273	-5.102820	-0.856647
H	4.551431	-3.982150	-1.543921
H	4.508768	-4.284410	0.218738
C	1.948015	-3.397805	0.697002
H	1.155789	-2.654076	0.857772
H	1.475236	-4.382039	0.529707
H	2.552054	-3.467543	1.619482
C	-9.263290	-1.030566	0.471744
H	-9.906259	-1.747522	0.995632
C	-0.717186	3.507583	-0.016813
C	1.995404	-2.984562	-1.813863
H	1.212128	-2.214897	-1.764788
H	2.635945	-2.772278	-2.688599
H	1.511369	-3.963437	-1.981021
C	-7.705860	0.787887	-0.842340
H	-7.144579	1.531745	-1.414084
C	-9.103977	0.812224	-0.884757
H	-9.617712	1.582500	-1.471792
C	0.705139	5.953728	0.007369
H	1.257925	6.898380	0.007986
C	0.717201	3.507582	0.017120
C	-3.883828	-4.150726	0.681710
H	-3.353349	-5.102679	0.857435
H	-4.551636	-3.981869	1.544253
H	-4.508686	-4.284548	-0.218327
C	-0.705137	5.953727	-0.006872
H	-1.257925	6.898378	-0.007403

[Mn(^{t}P3)]$^{-2}$

Mn	0.017351	0.779875	0.227941
O	1.401161	-0.536916	0.234872
O	-1.413701	-0.479588	0.503081
N	-1.267995	2.237094	0.136975
N	1.330624	2.227468	0.270896
N	9.902173	-0.120070	-0.725926
N	-9.775775	-0.119257	-1.304025
C	2.722461	-0.474137	0.058073
C	4.805697	0.854755	-0.122151
H	5.292536	1.835811	-0.157194
C	-2.731611	-0.402453	0.305924
C	7.039715	-0.249061	-0.425494
C	3.383039	0.830851	0.032323
C	4.893985	-1.565618	-0.275741
H	5.488206	-2.476053	-0.356408
C	-4.712750	0.866740	-0.472472
H	-5.147220	1.813896	-0.811868
C	3.494187	-1.670806	-0.118019
C	-3.321647	0.862365	-0.138863
C	5.569661	-0.312725	-0.273583
C	-2.574537	2.062717	-0.268141
H	-3.083498	2.928642	-0.712457
C	2.686790	2.065703	0.107682
H	3.287493	2.972888	-0.030931
C	-6.973108	-0.214581	-0.638230
C	7.805926	0.850225	0.044290
H	7.328957	1.684859	0.564560
C	-1.397667	4.717268	0.402207
H	-2.491221	4.724432	0.360027
C	7.786089	-1.280310	-1.052797
H	7.288396	-2.158760	-1.471407
C	-2.983257	-2.883286	1.037953
C	-7.925845	-1.086293	-0.048951
H	-7.626590	-1.816567	0.707197
C	-5.534623	-0.259473	-0.298372
C	9.175509	-1.172335	-1.173629
H	9.742162	-1.972131	-1.665161
C	2.814377	-3.063763	-0.132517
C	-3.569872	-1.548547	0.510358
C	-4.950078	-1.447224	0.222958
H	-5.584077	-2.323720	0.357142
C	1.424210	4.713010	0.602962
H	2.513060	4.729719	0.708086
C	9.193908	0.866902	-0.127192
H	9.777029	1.718481	0.243423
C	-1.938815	-3.436534	0.034932
H	-1.128268	-2.712846	-0.125209
H	-1.501371	-4.378570	0.413041
H	-2.411381	-3.653189	-0.940295
C	-2.317857	-2.658466	2.422215
H	-1.514129	-1.910384	2.361776
H	-3.061843	-2.309760	3.161108
H	-1.887298	-3.604019	2.800076
C	3.821736	-4.221977	-0.325102
H	3.270116	-5.178528	-0.337364
H	4.371567	-4.147642	-1.279406
H	4.559450	-4.279376	0.494246
C	2.082966	-3.318921	1.211378
H	1.323781	-2.548342	1.404301
H	1.586664	-4.306430	1.198062
H	2.801613	-3.316663	2.050965
C	-9.275478	-1.002806	-0.406308
H	-10.003642	-1.678161	0.058610
C	-0.700094	3.483814	0.300456
C	1.809100	-3.138234	-1.312701
H	1.050830	-2.345667	-1.240976
H	2.336011	-3.028984	-2.277902
H	1.293585	-4.115848	-1.320300
C	-7.502033	0.707924	-1.579949
H	-6.848050	1.405881	-2.109191
C	-8.870604	0.715812	-1.867758
H	-9.267599	1.429080	-2.600099
C	0.711192	5.917728	0.698103
H	1.252728	6.854855	0.866288
C	0.749547	3.481879	0.392588
C	-4.059017	-3.978688	1.228018
H	-3.575876	-4.892723	1.616096
H	-4.836409	-3.683841	1.954406
H	-4.557576	-4.249166	0.280896
C	-0.703561	5.920002	0.595504
H	-1.260623	6.858589	0.688541

Kinetic Data from Cyclic Voltammetry

It is possible to calculate meaningful kinetic data for the interaction of salen complex with CO_2 from reversible electrochemical processes. If there exists a reversible electron-transfer reaction that is followed by a fast electrochemical (or catalytic) reaction, the peak catalytic current (i_{cat}) is given by:

$$i_{cat} = n_{cat}FA[analyte](Dk_{cat}[Q]^{y})^{\frac{1}{2}} \quad \textbf{(1)}$$

where i_{cat} = peak catalytic current (mA/cm^2), n_{cat} = number of electrons required for the catalytic process, F = Faraday constant (C mol^{-1}), A = surface area of the working electrode (cm^2), [analyte] = analyte concentration (M), D = catalyst diffusion constant (cm^2 s^{-1}) and [Q] is the substrate coefficient.

It is therefore necessary to prove that the system obeys pseudo-first order kinetics to apply the above model. At a minimum, this requires proof that the reaction is first order in the analyte and the concentration of CO_2, and that the concentration of CO_2 is large in comparison to that of the analyte. It is also necessary to compare the peak currents for salen complexes in the presence of CO_2 with the absence of CO_2. If there exists a reversible electron transfer reaction that does not generate a chemically active species, the peak current (i_p) is given by:

$$i_p = 0.4463n_p^{\frac{3}{2}}FA[analyte]\left[\frac{F\nu D}{RT}\right]^{\frac{1}{2}} \quad \textbf{(2)}$$

where i_p = peak current (mA/cm^2), n_p= number of electrons required for the catalytic process, F= Faraday constant (C mol^{-1}), A = surface area of the working electrode (cm^2), [analyte] = analyte concentration (M), ν = scan rate (V s^{-1}), R = universal gas constant (J mol^{-1} K^{-1}) and T = temperature (K).

The combination of (1) and (2) yields an expression for k_{cat}[Q], or TOF, in terms of the $\frac{i_{cat}}{i_p}$ ratio, which can be directly examined from CV.

$$k[Q] = \frac{F\nu n_p^{\,3}}{RT}\left[\frac{0.4463}{n_{cat}}\right]^2\left[\frac{i_{cat}}{i_p}\right]^2 \quad \textbf{(3)}$$

where F = Faraday constant (C mol^{-1}), ν = scan rate (V s^{-1}), n_p = number of electrons facilitated by the redox process, R = universal gas constant (J mol^{-1} K^{-1}), T = temperature (K), n_{cat} = number of electrons facilitated in the catalytic transformation, i_{cat} = peak catalytic current (mA/cm^2), i_p = peak current under N_2 (mA/cm^2).

It is also possible to directly derive a CO_2 association constant directly from the Nernst equation by varying the concentration of CO_2, and observing how the position of the redox feature shifts, according to equation (4).

$$E = E^0 + \left(\frac{RT}{nF}\right)\ln\{1 + [CO_2]K_{CO2}\} \quad \textbf{(4)}$$

where E = observed process (V), R = universal gas constant (J mol^{-1} K^{-1}), T = temperature (K), n = number of electrons transferred, F = Faraday constant (C mol^{-1}), $[CO_2]$ = CO_2 concentration (M), K_{CO2} = CO_2 association constant (M^{-1})).

Application of the calculations to Mn^{t}P3Cl: The first reduction processes are reversible for **Mn^{t}P3Cl**; therefore, this mathematics can apply. Plotting the current density as a function of a number of parameters suggested that the reaction was first order in $[CO_2]$, second order in $[H^+]$ and first order in [analyte] (Figure S15). The reduction of CO_2 by **Mn^{t}P3Cl** shows that the reaction is both first order in [analyte] and $[CO_2]$, and the concentration of CO_2 (0.23 M in DMF) is in excess of the analyte (1 mM), while saturation is a property that may be observed in a system with favourable electrochemical behaviour.[9] The titration of TFE into the solution under an atmosphere of CO_2 resulted in an increase in the current density to a maximum at E_{pc} = –2.64 V *vs.* Fc^0/Fc^+. The addition of excess TFE after this point resulted in no observed change. This was also accompanied by the anodic shift of the process from E_{pc} = –2.31 to –2.16 V *vs.* Fc^0/Fc^+ which is indicative of CO_2 association.[10] In the absence of TFE for a solution of **Mn^{t}P3Cl** (1 mM), $\frac{i_{cat}}{i_p}$ is approximately 1, indicating that a proton source is needed to facilitate CO_2 reduction. The addition of TFE to **Mn^{t}P3Cl** under CO_2 resulted in a peak $\frac{i_{cat}}{i_p}$ of 7.33 and a TOF of 10.5 s^{-1} at 0.63 M TFE (for the evolution of CO). The changes in peak shape and position are characteristic of CO_2 association.[10] Values for K_{CO2} have been calculated from CV data in macrocycles, as reported by Gagne *et al*. and Fujita *et al.* using a variation of the Nernst equation.[11,12]

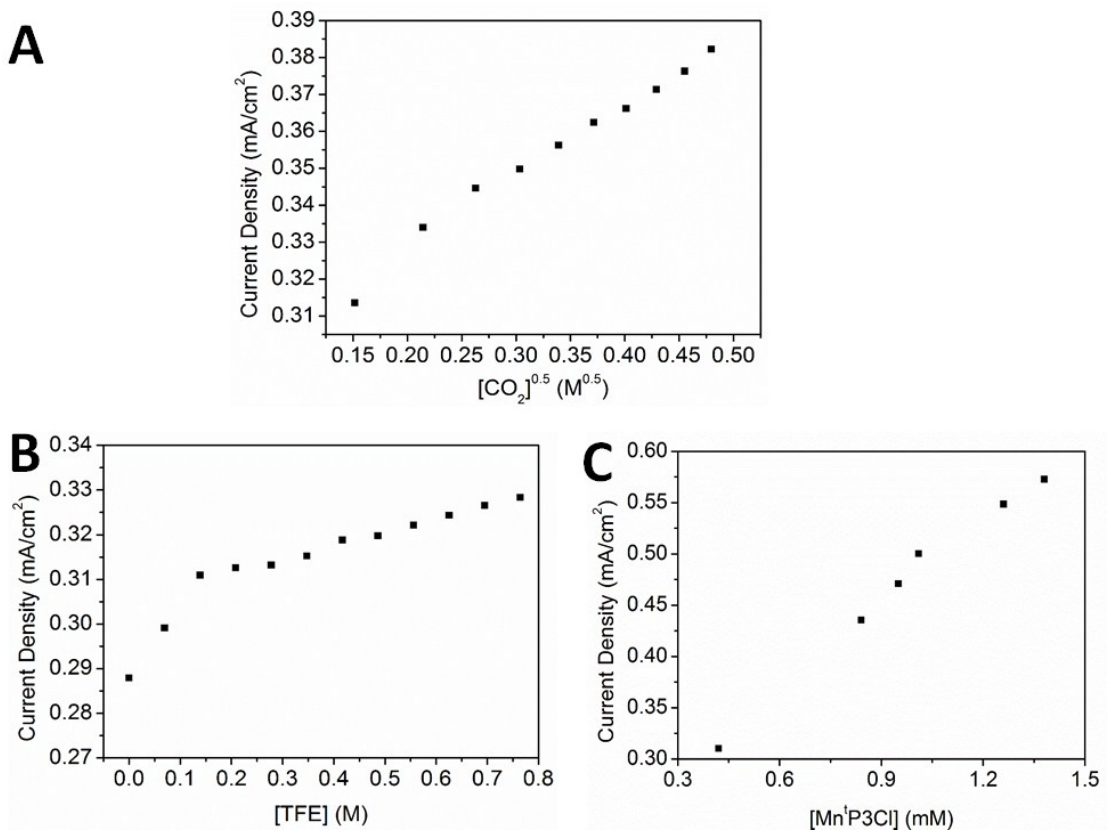

Figure S15. Plot of the current density (i_{cat}) of **Mn^{t}P3Cl** vs. **A** $[CO_2]^{0.5}$, demonstrating a first order kinetic relation in $[CO_2]$ **B** [TFE] under CO_2 saturation, demonstrating an initial second order kinetics relation in [TFE] prior to saturation and **C** vs. [**Mn^{t}P3Cl**] under CO_2 saturation, demonstrating a first order kinetic relation in [**Mn^{t}P3Cl**].

Application of the calculations to Mn^{t}P4Cl: The first reduction processes are reversible for **Mn^{t}P3Cl**; therefore, the aforementioned mathematics can apply. The effect of the electron donating groups on the bridging diamine were apparent when solution state CV experiments were performed on **Mn^{t}P4Cl** (1 mM) in 0.1 M [(n-C_4H_9)$_4$N]PF_6/DMF in the presence of CO_2, where favourable activity for the reduction of CO_2 was observed (Figure S16). The I_R redox process (corresponding to the Mn(III/II) reduction) was not significantly shifted from its **Mn^{t}P3Cl** analogue, remaining at $E_{½}$ = –0.55 V *vs*. Fc^0/Fc^+, with a slight cathodic shift in the presence of CO_2. The change of the peak shape from reversible to irreversible under a CO_2 atmosphere implies that there an affinity of the complex for CO_2. For the II_R ligand process at E_{pc} = –2.39 V *vs*. Fc^0/Fc^+, the small increase in current density and slight anodic shift compared to the analogous CV under an inert N_2 atmosphere are indicative of CO_2 association. With increasing TFE as a proton source (up to 0.55 M), the peak shifted anodically indicating CO_2 association. A second ligand based reduction, corresponding to a possible catalytic wave was not observed using DMF as the solvent. Titration of TFE into the electrochemical solvent under an atmosphere of CO_2 resulted in an anodic shift of the second ligand based reduction process from E_{pc} = –2.39 V (under N_2 saturation) to –2.27 V *vs.* Fc^0/Fc^+, indicative of CO_2 association,[10] with an average K_{CO2} of 12.7 ± 4.7 M^{-1}. This indicates weaker association compared with the **Mn^{t}P3Cl** analogue. The kinetics of the CO_2 interaction with **Mn^{t}P4Cl** were investigated using titration experiments revealing similar behaviour to **Mn^{t}P3Cl.** The reduction was found to be first order in CO_2, first order in [H^+], reaching saturation and first order in [analyte] (Figure S16).

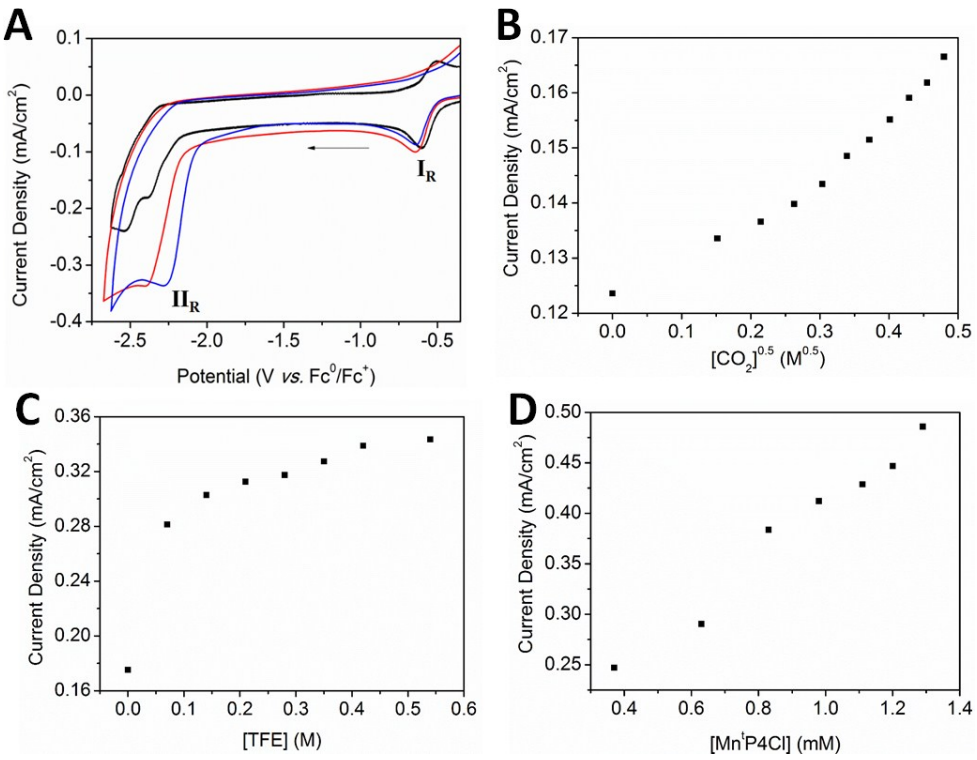

Figure S16. A Solution state CV showing the electrochemical response of **Mn^{t}P4Cl** (1 mM) under saturation conditions of N_2 (black), CO_2 (red) and CO_2 with TFE (5.5 mmol) as a proton source (blue) (0.1 M [(n-C_4H_9)$_4$N]PF_6/DMF as the supporting electrolyte, scan rate: 0.1 V s^{-1}, Fc (1 mM) was used as an internal standard). Plot of the current density (i_{cat})

of **Mn^{t}P4Cl B** vs. $[CO_2]^{0.}$, demonstrating a first order kinetic relation in $[CO_2]$. **C** vs. [TFE] under CO_2 saturation, demonstrating a second order kinetics relation in [TFE]. **D** vs. [**Mn^{t}P4Cl**] for solution state CV of **Mn^{t}P3Cl** under CO_2 saturation, demonstrating a first order kinetic relation in [**Mn^{t}P4Cl**].

CO_2 reduction studies

Solution state bulk electrolysis. Bulk electrolysis was performed in a custom threaded 60 mL single compartment cell with a custom airtight Teflon top, as reported by Kubiak *et al.*[13] The set-up consists of a carbon rod working electrode (surface area = 7.4 cm^2), a coiled Pt wire counter electrode protected from the bulk solution by fritted glass and an electrolysed Ag/AgCl pseudo reference, separated from solution by a CoralPor tip. The analyte solution (~40 mL) consisted of complex (1-2 mM) in 0.1 M $[(n\text{-}C_4H_9)_4N]PF_6$/MeCN/DMF (8:2). Prior to each experiment, the solution was purged with CO_2 for 20 min, with the chosen voltage determined by the CV experiments.

Product analysis: Gas phase analysis was performed by sampling 1 mL of the headspace of the cell at 20 min. intervals and injecting on a Hewlett-Packard 7890A series gas chromatograph with two molecular sieve columns (30 m × 0.53 mm i.d. × 25 μm film). The 1 mL injection was split between two columns, one with N_2 carrier gas and one with He carrier gas to quantify both CO and H_2 respectively. Prior to analysis, instrument specific calibration curves were used to determine the amount of each gas produced. Solution phase analysis was performed on the bulk solution to quantify formic acid production by sampling the bulk electrolysis solution (5 mL) after electrolysis. D_2O (1 mL) was added to the solution and this was well mixed, prior to its dilution with dichloromethane. The D_2O layer was separated prior to the addition of concentrated hydrochloric acid (1 drop). Samples were analysed by ^1H NMR and spectra were recorded on a Bruker AVANCE300 spectrometer operating at 300 MHz for ^1H. Spectra were recorded at 298 K. DMF was not used at highly cathodic potentials, since DMF is itself able to transform into CO or formic acid upon reduction.[14]

Chemical CO_2 reduction. The chemical reduction of CO_2 was achieved on **Mn^{t}P3Cl** under air free conditions through the one and two electron reduction of the analyte (1 mM in DMF) with one and two equivalents of cobaltocene in the presence of CO_2. FT-IR spectra were recorded on a Thermo Scientific Nicolet 6700 with a resolution of 4 cm^{-1}.

MnP2Cl MnP3Cl and MnP4Cl

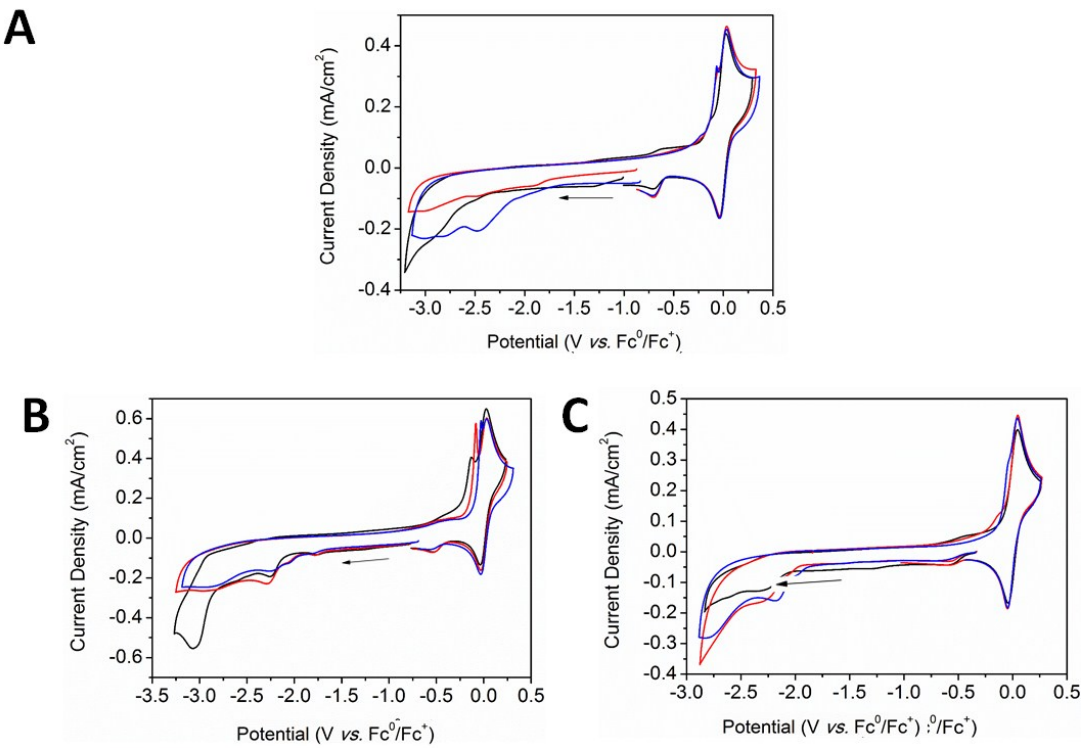

Figure S17. Solution state CV of **a) MnP2Cl** (1 mM) **b) MnP3Cl** (1 mM) and **c) MnP4Cl** (1 mM) under an atmosphere of N_2 (black), CO_2 (red) and CO_2 with saturated TFE (blue) (0.1 M $[(n\text{-}C_4H_9)_4N]PF_6$/DMF as the supporting electrolyte, scan rate: 0.1 V s^{-1}, Fc (1 mM) was used as an internal standard).

The instability of some Mn(III) salen metal complexes under reducing conditions in an inert N_2 atmosphere was reflected in their electrochemical response in the presence of CO_2. **MnP2Cl, MnP3Cl and MnP4Cl** demonstrated no significant electrochemical activity under a saturated CO_2 atmosphere. In fact, the presence of CO_2 resulted in a decrease in current density compared to the observed Faradaic redox processes under N_2 saturation (Figure S17).

Mn^{t}P1Cl: The generation of products from CO_2 is described in the main text.

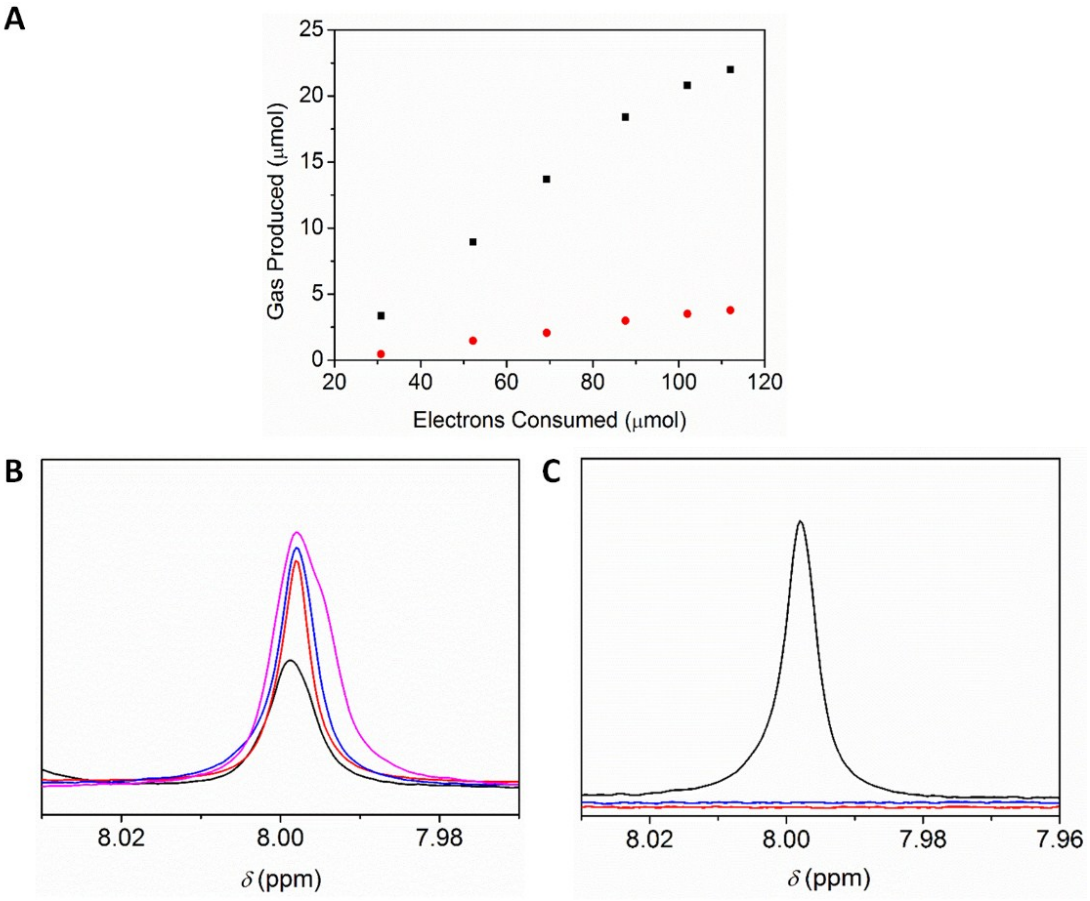

Figure S18. A Production of H_2 (black) and CO (red) from CO_2 by **Mn^{t}P1Cl** (1.12 mM) during CPE **B** ^{1}H NMR of the bulk electrolysis solution after work up from CPE in D_2O at 300 MHz under CO_2 saturation after 30 min (black), 60 min (red), 90 min (blue) and 120 min (pink); **C** under CO_2 saturation with **Mn^{t}P1Cl** (black), under CO_2 saturation without **Mn^{t}P1Cl** (red) and under N_2 saturation with **Mn^{t}P1Cl** (red). The peak at $\delta = 8.00$ ppm corresponds to the generation of formic acid. Spectra were referenced to D_2O.

MnP1Cl: This complex exhibited electrochemical activity in the presence of CO_2. Under CO_2 saturation, the I_R redox wave (corresponding to the Mn(III/II) process) became irreversible and shifted cathodically relative to the redox couple under N_2 (Figure S19A). The addition of a weak Brønsted acid, TFE, as a proton source under CO_2 saturation resulted in a cathodic shift of the Mn(III/II) process and a large anodic shift of the II_R redox process. This was accompanied by an increase in current density of the III_R feature at $E_{pc} = -2.75$ V *vs.* Fc^0/Fc^+. The current increases were attributed to the conversion of CO_2 into various products. The titration of the weak Brønsted acid into the reaction mixture under CO_2 saturation resulted in a linear increase of the current density, which is consistent with second order kinetics in TFE (Figure S19B).

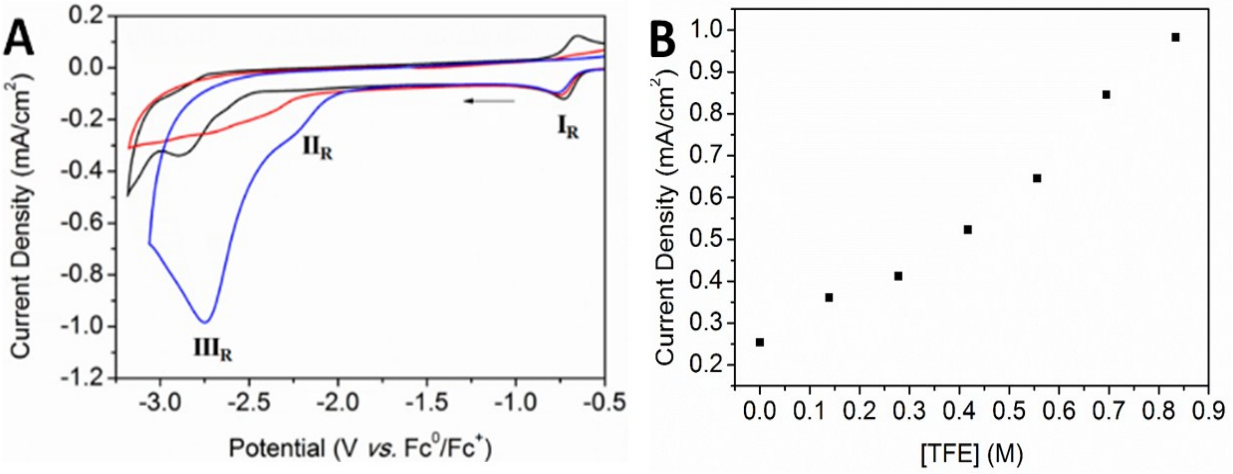

Figure S19. A Solution state CV showing the electrochemical response of **MnP1Cl** (1 mM) under saturation conditions of N_2 (black), CO_2 (red) and CO_2 with TFE (8 mmol) as a proton source (blue) (0.1 M $[(n\text{-}C_4H_9)_4N]PF_6$/DMF as the supporting electrolyte, scan rate: 0.1 V s^{-1}, Fc (1 mM) was used as an internal standard). **B** Plot of Current density (i_{cat}) vs. [TFE] for solution state CV of **MnP1Cl** (1 mM) under CO_2 saturation, demonstrating a second order kinetics relation in [TFE].

Bulk electrolysis was performed on **MnP1Cl** (1.12 mM) with TFE (0.7 M) as the proton source to analyse the gaseous CO_2 reduction products and to obtain information about the lifetime of the complex. CO was detected *via* gas chromatography (GC) and was accompanied by the generation of H_2 on the passing of 8.2 C of charge after 0.75 turnovers. The generation of H_2 and CO as a function of time decays over the course of 3 h (Figure S20A). The low Faradaic efficiency of the system and the deviation from linearity of the gas production suggests that degradation is occurring. Rapid loss of current density over the course of the bulk electrolysis experiment limited the amount of current passed to 8.2 C, which yielded a current density of 0.08 mA/cm^2. The bulk electrolysis solution was also analysed for additional liquid phase products *via* solution state ^{1}H NMR experiments. A low intensity peak at δ = 7.99 ppm, corresponding to formic acid, was observed in the NMR (Figure S20B). Blank bulk electrolysis experiments in the absence of both CO_2 and **MnP1Cl** were undertaken, in which a formic acid peak was not detected, suggesting that the formic acid was a result of the salen metal complex.

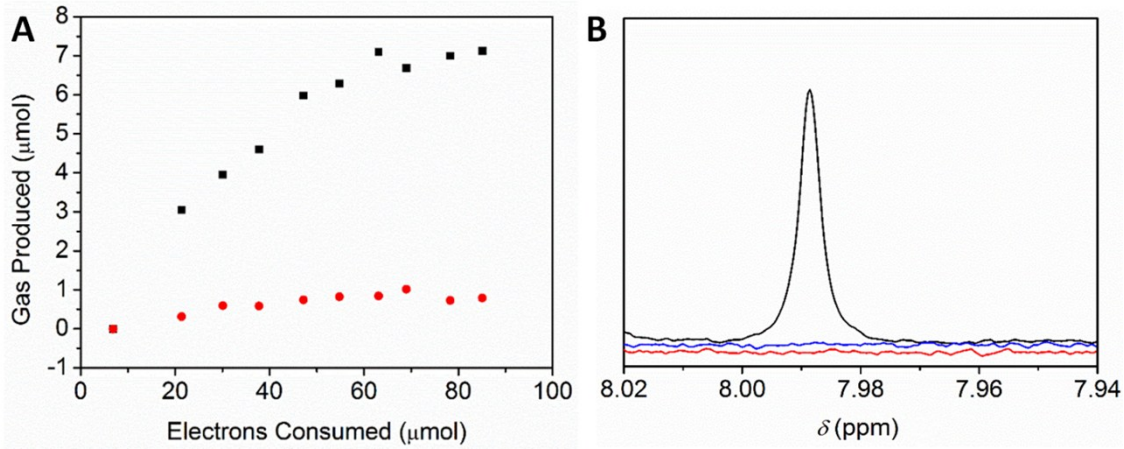

Figure S20. Production of H_2 (black) and CO (red) from CO_2 by **MnP1Cl** (1.12 mM) during CPE (0.1 M $[(n\text{-}C_4H_9)_4N]PF_6$/DMF/MeCN(8:2) with TFE (0.7 M) as the supporting electrolyte under CO_2, E_{pc} = –1.85 V vs. Ag/Ag^+). **b)** ^{1}H NMR of the bulk electrolysis solution (E_{pc} = –1.85 V vs. Ag/Ag^+) after work up from CPE in D_2O at 300 MHz under CO_2 saturation with **MnP1Cl** (black), under CO_2 saturation without **MnP1Cl** (red) and under N_2

saturation with **MnP1Cl** (blue). The peak at δ = 7.99 ppm corresponds to the generation of formic acid. The spectrum was referenced to D_2O.

Mn^{t}P2Cl: Initial solution state CV measurements on **Mn^{t}P2Cl** under both N_2 and CO_2 saturation showed its improved activity for the reduction of CO_2 over **Mn^{t}P1Cl.** In the presence of CO_2, there was a slight cathodic shift of the I_R process (corresponding to the Mn(III/II) reduction) at $E_{½}$ = –0.74 V *vs*. Fc^0/Fc^+ compared with its position under N_2 saturation (Figure S21A).[10] The current density of the process at $E_{½}$ = –2.57 V *vs*. Fc^0/Fc^+ continues to increase and shift anodically upon the addition of excess TFE. The processes that were observed in **Mn^{t}P2Cl** under N_2 at E_{pc} = –2.84 V, –2.95 V and –3.11 V *vs*. Fc^0/Fc^+ were not observed under CO_2. Titration of TFE into the solution of **Mn^{t}P2Cl** under CO_2 resulted in an increase in the current density at E_{pc} = –2.58 V *vs.* Fc^0/Fc^+ until a concentration of 0.2 M TFE. A linear plot of current density *vs.* [TFE] reveals that the reaction is initially consistent with second order kinetics in TFE; however, the addition of excess TFE causes a loss of current intensity, indicating that this particular complex may not be stable to excess TFE (Figure S21B).

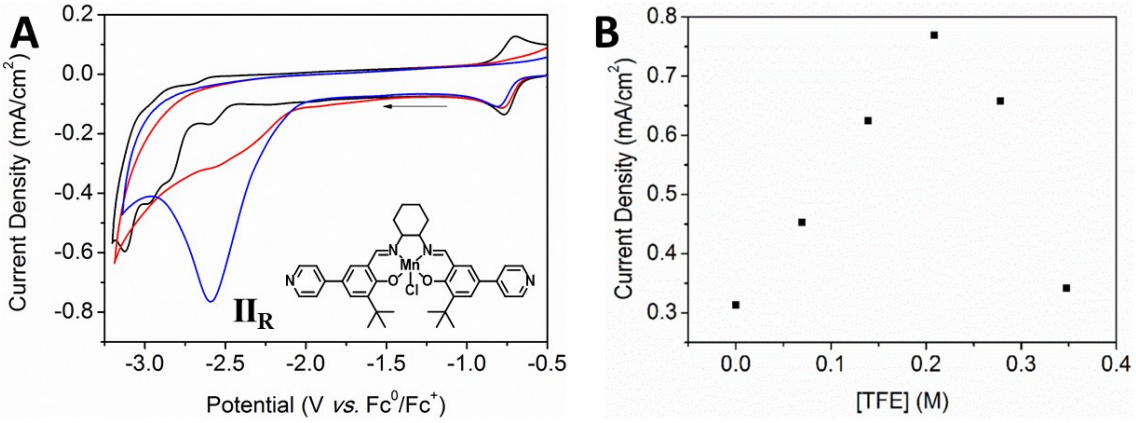

Figure S21. A Solution state CV showing the electrochemical response **A Mn^{t}P2Cl** (1 mM) under saturation conditions of N_2 (black), CO_2 (red) and CO_2 with TFE (2.1 mmol) as a proton source (blue). **B** Plot of current density (i_{cat}) vs. [TFE] for solution state CV of **Mn^{t}P2Cl** (1 mM) under CO_2 saturation, demonstrating a second order kinetics relation in [TFE].

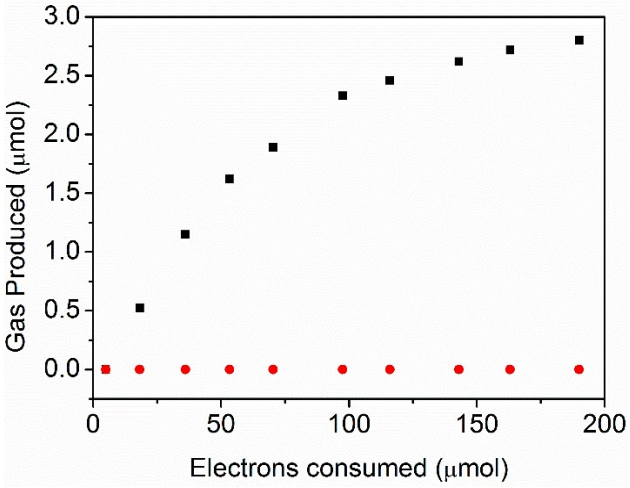

Figure S22. Production of H_2 (black) and CO (red) from CO_2 from **Mn^{t}P2Cl** (1.33 mM) with TFE (0.7 M) during CPE. 0.1 M $[(n\text{-}C_4H_9)_4N]PF_6$/MeCN (8:2) as the supporting electrolyte under CO_2. E_{pc} = –1.85 V vs. Ag/Ag^+.

Mn^{t}P3Cl: Given the promising electrochemical properties of **Mn^{t}P3Cl**, a chemical reduction was performed to generate the doubly reduced ligand species and the $\nu_{C=N}$ shift was monitored using IR (Figure S23). Upon the addition of CO_2, a slight shift in the imine stretch to lower wavenumbers and a decrease in intensity were observed. The shift in the $\nu_{C=N}$ upon the addition of two equivalents of cobaltocene was consistent with the changes observed in the IR SEC measurements; however, when CO_2 was introduced into a solution of the reduced species, the regeneration of the imine stretch was observed in the IR at $\nu_{C=N}$ = 1590 cm^{-1}.

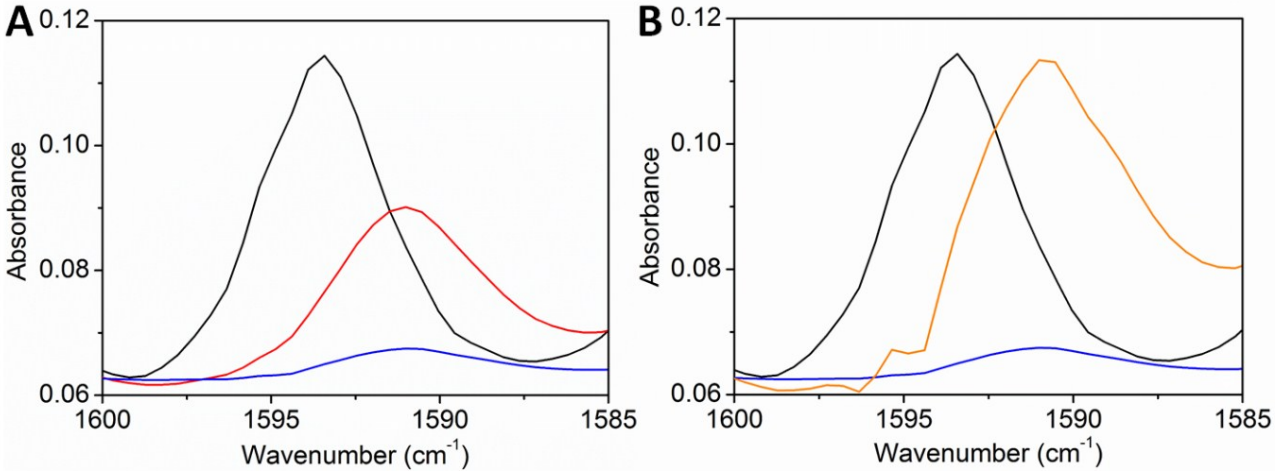

Figure S23. Solution state IR spectra of the chemical reduction of **Mn^{t}P3Cl** (4 mM) in DMF under N_2 **A** prior to the addition of cobaltocene (black), on the addition of cobaltocene (1 eq.-red, 2 eq.-blue), **B** prior to the addition of cobaltocene under N_2 (black), on the addition of cobaltocene (2 eq.) under N_2 (blue) and after the addition of excess CO_2 on the doubly reduced **Mn^{t}P3Cl** species (orange).

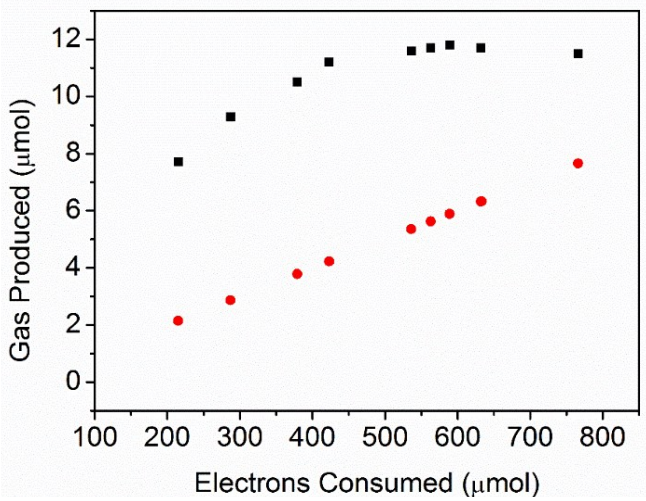

Figure S24. Production of H_2 (black) and CO (red) from CO_2 from **Mn^{t}P3Cl** (1.15 mM) with TFE (0.63 M) during CPE. 0.1 M [(n-C_4H_9)$_4$N]PF_6/MeCN (8:2) as the supporting electrolyte under CO_2. E_{pc} = –1.85 V vs. Ag/Ag$^+$.

Mn^{t}P4Cl: As was observed in the case of **Mn^{t}P3Cl,** the processes occurring at high cathodic potentials in **Mn^{t}P4Cl** (1.26 mM) with TFE (0.55 M) at E_{pc} = –2.25 V *vs*. Fc^0/Fc could not be easily evaluated. A lower Faradaic efficiency of both CO and H_2 was calculated, as measured over 3 h from the first 2.56 turnovers of the analyte (Figure S25)**.** A linear relationship in the production of CO was initially maintained; however this plateaus, indicating that the electrochemical properties of the salen may be short-lived.

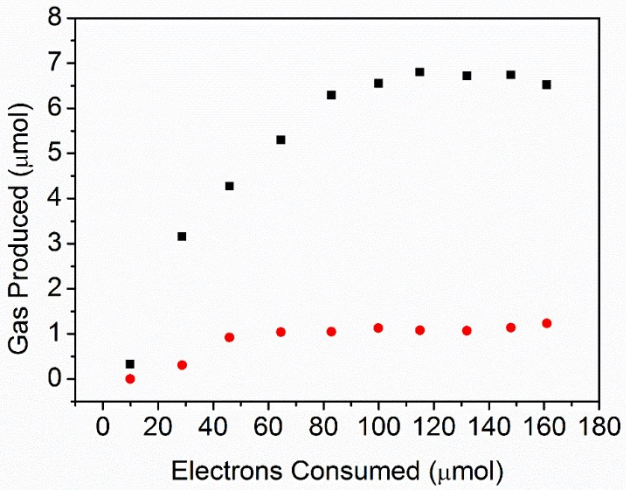

Figure S25. Production of H_2 (black) and CO (red) from CO_2 from **Mn^{t}P4Cl** (1.26 mM) with TFE (0.55 M) during CPE. 0.1 M $[(n\text{-}C_4H_9)_4N]PF_6$/MeCN (8:2) as the supporting electrolyte under CO_2. E_{pc} = −1.85 V vs. Ag/Ag^+.

Table S2. Faradaic Efficiencies for the generation of H_2 and the conversion of CO_2 into CO and HCOOH. All experiments were performed in (0.1 M $[(n\text{-}C_4H_9)_4N]PF_6$/DMF/MeCN (8:2) with TFE as the supporting electrolyte under CO_2, E_{pc} = −1.85 V vs. Ag/Ag^+).

Experiment	F_{CO} (%)	F_{H2} (%)
Solvent	0	0
Solvent + TFE (0.7 M)	0	12
MnP1Cl +TFE (0.7 M)	4	30
Mn^{t}P1Cl + TFE (0.7 M)	8	40
Mn^{t}P1Cl under N_2	1	15
Mn^{t}P2Cl + TFE (0.32 M)	0	14
Mn^{t}P3Cl + TFE (0.63 M)	6	20
Mn^{t}P4Cl +TFE (0.55 M)	4	13

References

1. N. Gisch, J. Balzarini and C. Meier, *J. Med. Chem.*, 2007, **50**, 1658-1667.
2. S. K. Murphy, D. A. Petrone, M. M. Coulter and V. M. Dong, *Org. Lett.*, 2011, **13**, 6216-6219.
3. G. A. Morris and S. T. Nguyen, *Tetrahedron Lett.*, 2001, **42**, 2093-2096.
4. G. A. Morris, H. Zhou, C. L. Stern and S. T. Nguyen, *Inorg. Chem.*, 2001, **40**, 3222-3227.
5. S.-H. Cho, B. Ma, S. T. Nguyen, J. T. Hupp and T. E. Albrecht-Schmitt, *Chem. Commun.*, 2006, **42**, 2563-2565.
6. S.-S. Sun, C. L. Stern, S. T. Nguyen and J. T. Hupp, *J. Am. Chem. Soc.*, 2004, **126**, 6314-6326.
7. M. P. Feth, C. Bolm, J. P. Hildebrand, M. Köhler, O. Beckmann, M. Bauer, R. Ramamonjisoa and H. Bertagnolli, *Chem. Eur. J.*, 2003, **9**, 1348-1359.
8. L. D. Field, S. S and J. R. Kalman, *Organic Structures from Spectra*, John Wiley and Sons, West Sussex, 4th edn., 2011.
9. S. Ašperger, in *Chemical Kinetics and Inorganic Reaction Mechanisms*, Springer US, Boston, MA, 2003, pp. 3-103.
10. R. R. Gagne, J. L. Allison, D. M. Ingle, *Inorg. Chem.* 1979, **18**, 2767-2774.
11. E. Fujita, C. Creutz, N. Sutin, D. J. Szalda, *J. Am. Chem. Soc.* 1991, **113**, 343-353.

12. R. R. Gagne, D. M. Ingle, *J. Am. Chem. Soc.* 1980, **102**, 1444-1446.
13. M. L. Clark, B. Rudshteyn, A. Ge, S. A. Chabolla, C. W. Machan, B. T. Psciuk, J. Song, G. Canzi, T. Lian, V. S. Batista, C. P. Kubiak, *J. Phys. Chem. C* 2016, **120**, 1657-1665.
14. M. Chiba, M. N. Thanh, Y. Hasegawa, Y. Obora, H. Kawasaki, T. Yonezawa, *J. Mater. Chem. C.* 2015, **3**, 514-520.